COMPARISON OF ITERATIVE CLOSEST POINT (ICP) AND THIN-PLATE SPLINES METHODS FOR THE 3-D IMAGE REGISTRATION

by

İSMAİL BURAK PARLAK

B.S., in Computer Engineering, Galatasaray University, 2001

Submitted to the Institute of Biomedical Engineering
in partial fulfillment of the requirements
for the degree of
Master of Science
in
Biomedical Engineering

Boğaziçi University
2005

ACKNOWLEDGMENTS

I am deeply grateful to my thesis supervisors, Assoc. Prof. Dr. Ahmet ADEMOĞLU and Assoc. Prof. Dr. Cengizhan ÖZTÜRK for their academic supports and friendly tolerances. I gratefully acknowledge the invaluable encouragements of Uzay Emrah EMİR and Serhan KALSIN.

I wish to thank Haris SAYBAŞILI and Temel ÖNCAN for their friendships and precious moral supports. I also deeply appreciate the invaluable assistance and discussions with Assoc. Prof. Dr. Önder KORFALI.

Finally, very special thanks are destined to my parents. I am indebted them for their encouragements, their great motivations and especially for their inspirations.

ABSTRACT

COMPARISON OF ITERATIVE CLOSEST POINT (ICP) AND THIN-PLATE SPLINES METHODS FOR THE 3-D IMAGE REGISTRATION

In medical image registration, algorithm choice and its application on images depend on the localization and where and how images are acquired. In this study, a linear algorithm; Iterative Close Point and an elastic method; Thin-Plate Splines are used to register volumes obtained from different sensors. For the sake of 3-D image registration, their performance on different modalities are compared on MATLAB environment. This study shows the registration results of 5 different modalities; T1, T2, PD - weighted MR, PET and SPECT images. The slice information is collected for volume reconstruction and a 3-D Registration is implemented. Thin-Plate Splines efficiency is studied according to landmark numbers. The simulation is presented as the mean of 20 experiments for point pair measurements and registration results are compared with respect to Mean Distance Difference and Root Mean Square Analysis. The measurements on skull surface represent that Thin Plate Splines (TPS) gives better results than Iterative Closest Point (ICP) Algorithm for less landmarks. Nevertheless, we observed that ICP that does not necessitate landmarks in the measurements gives better registration results in case where TPS measurements are implemented with more reference points.

Keywords: Image Registration, Thin-Plate Splines, Morphometrics, Iterative Closest Point Algorithm, Multimodality Image Analysis.

ÖZET

YİNELEYİCİ YAKIN NOKTA (YYN) VE İNCE PLAKA İŞLEVLERİ (İPİ) METODLARININ 3-B GÖRÜNTÜ ÇAKIŞTIRILMASINDA KARŞILAŞTIRILMASI

Tıbbi görüntüleri çakıştırmada kullanılacak algoritmanın seçimi ve uygulamaları, radyolojik görüntülerin yerine ve nerede, nasıl çekildiğine bağlıdır. Bu çalışmada, farklı algılayıcılar tarafından çekilmiş hacimleri çakıştırmada doğrusal Yineleyici Yakın Nokta Algoritması ve elastik İnce Plaka Splin İşlevleri metodu kullanılmıştır. 3-B görüntü çakıştırma için, yöntemlerin performansları bu farklı biçimler için MATLAB platformunda karşılaştırılmıştır. Bu çalışma 5 farklı biçimin; T1, T2 ve PD ağırlıklı MR, PET ve SPECT çakıştırma sonuçlarını göstermektedir. Hacim oluşturmada kesit bilgisi toplanmış ve 3-B çakıştırma uygulanmıştır. İnce Plaka Splin İşlevlerinin etkinliği referans nokta sayısına bağlı olarak incelenmiştir. Benzetimde nokta çifti ölçümleri 20 deneyin ortalaması olarak gösterilmiş ve çakıştırma sonuçları Ortalama Uzaklık Farkı ve Ortalama Karesinin Karekökü Analiziyle karşılaştırılmıştır. Kafatası yüzeyinde yapılan ölçümler referans nokta sayısı az olduğunda İnce Plaka Splin İşlevlerinin (İPİ) , Yineleyici Yakın Nokta (YYN) Algoritmasına göre daha iyi sonuçlar verdiğini göstermektedir. Bununla beraber referans noktalara ihtiyaç duymayan YYN Algoritmasının ölçümlerde daha fazla referans noktası kullanılarak yapılan İPİ ölçümlerine göre daha başarılı çakıştırma sonuçları verdiği gözlenmiştir.

Anahtar Sözcükler: Görüntü Çakıştırma, İnce Plaka Splin İşlevleri, Morfometrik, Yineleyici Yakın Nokta Algoritması, Çok Biçimli Görüntü Analizi.

TABLE OF CONTENTS

LIST OF FIGURES

LIST OF TABLES

LIST OF SYMBOLS

P	Template or Source point sets in ICP
X	Target point sets in ICP
$d(p_i, x_j)$	Euclidean distance between two points
C	Mathematical operator that calculates closest point sets in ICP
Y	Closest point sets in ICP
q_r	3-D Rotation vector for a quaternion
q_t	3-D Translation vector for a quaternion
$R(q_R)$	Rotation matrix that corresponds to a certain quaternion
q	A single registration vector composed of rotation and translation
$f(q)$	Mean square error function for ICP
μ_P, μ_Y	Centers of mass of template and closest sets in ICP
$\phi(x, y, z)$	Trivariate function of the interpolating Thin-Plate Spline
$\theta(s)$	Radial Basis Function for a Thin-Plate Spline
Q	Template Landmarks in TPS
P	Target Landmarks in TPS
K	Displacement between corresponding landmarks in TPS
E	Bending Energy Function for a Thin-plate spline
ρ	Euclidean distance function in TPS
S_e	Global matrix constructed via control points coordinates
$R(x)$	Root Mean Square Function

LIST OF ABBREVIATIONS

CT	Computed Tomography
CTA	Computed Tomography Angiography
DSA	Digital Substraction Angiography
fMRI	Functional Magnetic Resonance Imaging
ICP	Iterative Closest Point
MRA	Magnetic Resonance Angiography
MRI	Magnetic Resonance Imaging
MSE	Mean Squared Error
NN	Nearest Neighbor
PD	Proton Density
PET	Positron Emission Tomography
RMS	Root Mean Square
ROI	Region of Interest
SPECT	Single Photon Emission Computerized Tomography
TPS	Thin-Plate Splines
VOI	Volume of Interest

1. IMAGE REGISTRATION

1.1 Introduction

In Image Processing, Image Registration and Fusion appear as necessary stages for applications like medical imaging, serial and satellite imaging, quality control, robot vision, vehicle or robot guidance.

In a nutshell, image registration is the process of alignment of images so that corresponding features can easily be superimposed and therefore related. A two or three dimensional image analysis; registration is briefly a series of operations applied in one of the sets in order to match *template* (also called as *source*) with *target.*

From an operational view, the inputs of registration are the two views to be aligned; the output is a geometrical transformation, which is merely a *mathematical mapping* from points in one view to points in the second. To the extent that corresponding points are mapped together, the registration is successful.

The need to register images has arisen in many practical problems in diverse fields. Historically, the main application area of registration was remotely sensed data at the end of 70s and first-half of 80s. Thanks to computer technology and especially sophisticated software implementations, new application areas are discovered for images registration. In her article Brown [1] divided image registration applications in 3 different areas; this classification is still valid for understanding current application domains;

1. **Computer Vision and Pattern Recognition**; for numerous different tasks such as segmentation, object recognition, shape reconstruction, motion tracking, stereo mapping, and character recognition.

2. **Medical Image Analysis**; including diagnostic medical imaging, such as tumor detection and disease localization and biomedical research including classification of microscopic images of blood cells, retinal examination, cervical smears and chromosomes.

3. **Remotely Sensed Data Processing**; for civilian and military applications in agriculture, geology, oceanography, oil and mineral exploration, pollution and urban studies, forestry and target location and identification.

At the same time, Besl [2] studied geometric modeling and the general cases for surface matching and implementation according to the similar historical aspects. He introduced also computerized approaches such as curve representations, point sets, curve and volume modeling. This article presents a good initiation to comprehend the ICP methodology prepared by the same author.

For medical image registration, the importance of alignment is due to coregistration between anatomical and structural volumes. It is clear that the invention of Functional Magnetic Resonance Imaging (fMRI) and new researches on Single Photon Emission Computerized Tomography (SPECT) and Positron Emission Tomography (PET) have emphasized the requirement of alignment. One of these actual researches is the study of Modern Brain Mapping.

The first brain activation studies harnessed the ability to take images of brain function, successively within the same scanning session. This was facilitated by the use of short half-life radio tracers using Positron Emission Tomography (PET). These techniques became available in the late 80s and the first reports of human brain activation studies appeared in 1988. Up until this time, regional differences among brain scans had been characterized in terms of hand-drawn regions of interest, reducing hundreds of thousands of voxels to a handful of Region of Interest (ROI) measurements, with a somewhat imprecise anatomical validity.

There were important developments in the early 90s that made the development

of fMRI very useful. This was a growing appreciation that functional specialization and regionally specific activations were not the complete story in discerning functional brain architectures. There was an increasing interest in functional integration and understanding the discourse among different brain areas during the execution of a sensori motor or cognitive process. This was reflected in attempts to take the characterization of functional imaging time series beyond the mass univariate approach to explicit multi-variate approaches that could look at the coupling among brain areas.

The determination of the correspondence between inter- or intra- modal images is a problem specific to the domain of objects being imaged, which is, in our thesis, **Human Brain**. To make the registration beneficial in medical diagnosis or treatment, the mapping that it produces must be applied in some clinically meaningful way by a system that will typically include registration as a subsystem. The larger system may combine the two registered images by producing a reoriented version of one view that can be **fused** with the other.

By the way, no registration is needed between two images if both the following conditions are satisfied;

- The same objects of study are observable in both images and they do not change shape.
- The relationship among them and to the image coordinate system does not change.

For any objects, even static or rigid, in any body region, these conditions are difficult to fulfill, and therefore, registration becomes necessary in medical image analysis.

These following terms; *registration*, *co-registration* and *normalization* are frequently used in publications. Nevertheless, their technical meanings are confused according to the interpretations. The term *normalization* is usually restricted to the

intersubject registration situation, and *registration* and *co-registration* are often used interchangeably. The algorithms used for all these applications have many features in common, so we prefer to use the term registration.

By the way, as another example to registration motion estimation is now a crucial step for the analysis of images sequences. We can view motion analysis as an image registration task with a fixed computational theory. Szeliski et al. [3] presented a new registration algorithm based on spline representations. A general scheme of motion estimation in medical imaging can cover local flow, global (parametric) flow or rigid flow resulting from camera motion. An interpretation of medical motion estimation is well introduced by Ozturk et al. [4] from MRI Data in cardiac imaging. Motion estimation is usually indispensable for soft tissue investigation and dynamic imaging of the musculoskeletal system.

In our study, our main goal is to register multimodal images by simulating artifacts due to patients lying on the gantry table with our protocols using the techniques which will be introduced in *METHODOLOGY* section. Firstly, to simulate these registration procedures we tried to use 3-D volumes based on head movements with different angles. Secondly, we aimed to compare the efficiency of two surface based methods through Mean Values of Distance Differences and Root Mean Square Analysis. Finally, we intended to measure the efficiency of landmark distribution on the patient skull for Thin-Plate Splines (TPS).

The dimensionality is one of the key points in alignment. Matching can be performed in any dimension. A 1-D method may perform a temporal match on a time series of spatially-consistent images. In 2-D methods, projection images or tomographic slices of different recordings are aligned, assuming that the images are made exactly in the same plane relative to the patient. 3-D methods consider a tomographic image not as a set of individual slices but as a volumetric data set that can be registered with another volume. Methods may include time as extra dimension; matching time series of 2-D images then becomes a 3-D method, matching of a time series of volumetric data becomes a 4-D method. In this study only 3-D spatial matching will be taken into

account. By the way, as an introduction, the theory in 2-D case will also be considered for TPS.

1.2 Image Modality

Volumetric biomedical images present a challenging variety of applications for spatial image coregistration. From the reconstruction of serial section images, to real-time integration of intraoperative video images with pre-acquired Magnetic Resonance and SPECT images, the full scientific, medical, and educational value of multidimensional biomedical images requires the detection, measurement and correction of errors in spatial alignment.

1.2.1 Unimodal Alignment

The reconstruction of 3-D structures from serial sections requires precise alignment of each section to its neighbors. Adjacent serial sections cannot be manually aligned directly on the stage of the digitizing sensor with the accuracy required for volume visualization and analysis, so the digital images must be coregistered mathematically.

Because of the large number of sections in a typical study, some automated method of section-to-section alignment must be used, even if the method occasionally fails. This approach is also introduced in Statistical Parametric Mapping (SPM) software package developed in the Department of Neurology at the University College of London to coregister multimodal slices. Correcting as many as 20% of the automated registrations is far less time consuming than manually coregistering the entire volume of sections. Because the individual sections are not identical, it is often difficult to unambiguously choose the proper registration, and the sections have been subjected to differing motions during staining and mounting, there remain elastic deformations

between sections that cannot be resolved by rigid transformations.

Volumetric unimodal registration is required to use medical images quantitatively to study disease progression, monitor patient response to treatment, and evaluate surgical performance for quality control. The reduction of tumor size due to chemotherapy or radiotherapy can be qualitatively assessed by viewing the pretreatment and posttreatment concurrently, and the change in total volume can be measured without spatially coregistering the image volumes, but the detailed progression and regression of the tumor can only be evaluated by exact registration of time series image volumes.

1.2.2 Multimodal Alignment

In Image Registration, information is typically provided by several images or aspects of a scene. They may come from different sensors, obtained using different imaging techniques or with different acquisition parameters or at different times. By the way, the heterogeneity of data and the complexity should be taken into account when we align them. These characteristics provide different aspects and different points of view on the problem by exploiting different physical properties. Especially, when a surgical operation is planned, the required data can be as heterogenous as **anatomical images**, **angiographic images**, **functional images** and occasionally **physiological signals**.

The registration of biomedical images obtained from different modalities presents both greater challenges and greater potential rewards. By combining information contained in multiple images of complementary modalities, synergism is achieved as voxel-by-voxel tissue characteristics can be determined with greater subtlety and precision than in any of the individual images. By combining structural with functional images, the relation of structure to function is revealed, thereby facilating the planning and delivery of effective medical intervention.

Medical images are widely used in health care and biomedical research; a very wide range of imaging modalities is now available. By the way, each modality contains different information in order to interpret and comment the data extracted from the same source and also from the same localization. As a result, we need to combine this amount of information in a framework to compare and visualize same pixels or voxels. To combine these sets, there are several methods according to their morphological or pixelwise properties.

Color analysis is a commonly encountered example of multiple band data in which the bands are inherently coregistered. Each voxel in a color image is represented by an RGB color vector, which contains more information than the scalar-valued voxel of a gray scale image. The color image may be considered a combination of red, green, and blue image bands in perfect physical registration. When a multicolor strain is used on a tissue section and imaged through a digital color sensor, the color image provides both a rich visual experience, in which several different structures may be easily identified by their color, as well as a rich vector data field of gross and subtle color differences from which structures can be automatically segmented. By retroactively coregistering images that capture different properties of the same subject, the same enhanced visual experience and analysis frame work may be used to advantage.

Optical stains for different tissue components can be applied to adjacent sections, the digitized sectional images coregistered, and the pair treated as a "two-band" multimodal image (or even six band if both images are color). Two- or three-band monochrome images can be easily displayed as pseudocolor images, and automated analysis can use any arbitrary number of image bands. Stokking et al. [5] proposed a similar approach for functional and anatomical brain surface fusion. In the article, HSV color model is used for the interpretation of 3D images retrieved from monochromatic sources.

Imaging modalities employed in our thesis can be grouped into two global categories: anatomical and functional. Anatomical modalities which depict primarily the patient morphology include X-Ray, CT (Computed Tomography), MR (Magnetic Res-

onance) and US (Ultrasound). In this study of registration simulation; we utilized only MR sub-modalities; T1-, T2- and PD- weighted MR slices.

Moreover, image modalities such as CT and MR imaging provide also complementary information for localization and characterization of tumors and normal tissues. Precise methods for image registration are required such that MR can be integrated with CT for accurate radiotherapy planning. A combination of MR and CT in cardiographic slices would give powerful results to characterize the disease and estimate the efficient treatment [6]. On the other hand, some prominent derivative techniques are so detached from the original modalities that they appear under a separate name, e.g. Magnetic Resonance Angiography (MRA), Digital Substraction Angiography (DSA), Computed Tomography Angiography (CTA) and Doppler Ultrasound. Furthermore, functional modalities which depict primarily information on the metabolism of the underlying anatomy include (planar) scintigraphy, SPECT, PET which together make up the nuclear medicine imaging modalities and fMRI. Also in our simulation work, we considered two of them; PET and SPECT to have functional information about the same patient.

Since information gained from two images acquired in the clinical track of events is usually of a complementary nature, proper integration of useful data obtained from the separate images is often desired. A first step in this integration process is to bring the modalities involved into spatial alignment, a procedure referred to as registration. After registration, generally a fusion step is preferred for the integrated display of the data involved. However, frequently these terms are confused and registration and fusion are considered as a unique step. In our work, we only register medical images in three dimensions and only the surface information will be taken into account.

For the same reasons, a PET (or fMRI) and MR registration and consequently multimodal fusion is becoming increasingly important in the interpretation of functional imaging [7]. To be fully effective, the activity represented by the PET image must be placed in the context of its anatomical location. Specific applications related with these principles include;

- Correlation of the brain glucose utilization with cortical atrophy demonstrated by T2-weighted MR images.
- Activation studies designed to map the function of the human cortex in vivo. Cortical activity patterns need to be correlated accurately with topographical location within a given gyrus.
- Studies monitoring drug treatment or the progress of the disease. Since longitudinal studies require comparison of images taken at different stages of the disease, detection of regional changes can be possible only after image registration.

1.2.3 Applications of Multimodal Registration

The ability to coregister images from multiple modalities or from multiple examinations allows the development of true data fusion to support both 2D and 3D visualization techniques. Using post-processing coregistration we can produce similar fused images that allow identification of anatomy from CT or MR imaging with overlays of data from PET or SPECT. Since these data acquisitions are 3D in nature we can visualize these fused data using standard 3D visualization techniques to demonstrate separate tissue components or illustrate the complementary information. Such combined images allow improved 3D image interpretation and are of particular use in surgical planning applications.

Moreover, in clinical applications the utilization of robots or the surgical assessment with intelligent devices requires coherent integration of spatial image data with sensing and actuating devices, each of them having its own coordinate system. According to the methodology introduced in [8], it is demonstrated that in robot-assisted surgery either the surface matching or other information about the images to be registered the accurate estimation of the geometric relationships is crucial.

The techniques of automated image coregistration were first applied to medical data sets to improve the stability of data analysis in functional magnetic resonance

imaging. Functional MR techniques for the measurement of brain activation, cerebral perfusion and capillary permeability rely on the analysis of multiple images collected over a period of 2-60 min. All these analysis techniques perform calculations on a pixel by pixel basis which use the signal intensity changes in the pixel which occur over time. In all cases the presence of movement - a spatial distortion in the data set means that the time course change may represent the movement of structures through the sample space rather than physiologically induced signal changes. This is of particular importance in Blood Oxygen Level Dependent (BOLD) fMRI where data collections tend to be long lasting and the subject is often performing cognitive or motor tasks that produce motion.

Another application of data coregistration is to allow comparison of apparently similar examinations to improve the detection of small structural changes. The use of an automated coregistration technique will allow generation of matching images with sub-voxel accuracy, which can then be directly compared. This process assumes that the differences between the images will not affect the accuracy of the coregistration process. Where changes are small, affect only a small volume of data and do not occur in areas of strong edge strength this assumption appears to be true. This allows visualization of changes due to brain atrophy, tumor growth or other processes where the change between the images is too small to be appreciated by eye. The interpretation of subtraction images is quite difficult since changes may be caused by either failure of coregistration, changes in intensity or movements of tissue boundaries. In addition the magnitude of the differences in the subtraction images can be small, making them difficult to identify.

On the other hand, the accuracy of automated coregistration algorithms can be utilized directly to allow measurement of the small volume changes that occur due to atrophic brain diseases. Using an accurate coregistration technique will produce images with no features in the brain except in the areas where the brain edge has moved due to atrophy. The volume change can be expressed as the appropriate fraction of the voxel volume. This technique has been applied to the brain of patients with Alzheimer's disease and allows detection of hippocampal atrophy in only 6 months.

Furthermore, the technique can also be used to measure volume changes due to other pathological processes such as tumors and also it can be extended to other medical approaches. Chen et al. [9] performed a 3D fusion to study the spinal cord and nerve root fusion and introduced the comparison of small multimodal changes between successive examinations.

Techniques for 3D image coregistration are becoming far faster as algorithmic improvements are developed. This has led several manufacturers to experiment with systems to allow automated prescription of the scanning geometry in MR imaging based on previously acquired images. When a patient attends for a follow-up scan the system will perform a relatively detailed survey scan. This survey will be coregistered to the scan performed on the previous visit and the transformation matrix will be used to adjust the scanning parameters. In theory, this should allow the follow-up scan to be acquired in a geometry already coregistered to the original examination. In practice, there remain some logistical problems in 3D and 4D with this approach and it is not clear how practical it will be to obtain sub-pixel/voxel coregistered examinations of large anatomical data set.

In the following papers; Nyúl et al. [10] and Holden et al. [11] have introduced relatively new methods based on voxel similarity measurements applied on multimodal and especially inter-subject MR slices. The utilization of similarity measurement built-on rigid body registration would provide good results. On the other hand, 3D statistical approaches would provide also considerable registrations. The likelihood maximization of Zhu et al. [12] introduced a newer SPECT-MR multimodal registration and stated a comparison between mutual information collection and new approach. Especially, in fMRI experiments the voxel similarity measurement is of considerable benefit, allowing the image prescription to track the movements of the head as the experiment is performed. Although this does not remove the need to coregister the data, it does mean that the amount by which the images need to be transposed is minimized and is of similar magnitude for all images.

Another recent study based on mutual information has been achieved by Rohlf-

ing et al. [13]. They studied MRI and fMRI registration using corresponding mutual information in navigated neurosurgery and measured the accuracy on the fused images. In a real-time environment, the data coming from OR would be registered with the recent images collected before surgery. Especially in stereotactic neurosurgery, this step becomes crucial and screws located on the rigid frame are considered like reference points.

Another application area of registration is video imaging or streaming. Video images are often acquired during surgery, for example using endoscopes or microscopes. For the same purpose of image guidance, it can be useful to relate the video images to preoperatively acquired diagnostic images. Video images are, like radiographs and many nuclear medicine images, projections. They differ, however, in that they normally only contain information about the surface of structures in the field of view, rather than a superposition of overlying structures. There is a lot of studies in computer vision literature on estimating 3-D shapes from one or more video camera views. Video images can be aligned with tomographic images either by first extracting surface structures, or directly.

2. METHODOLOGY

In this research, we suggested to compare two different surface-based methods; Iterative Closest Point (ICP) Algorithm and Thin-Plate Splines (TPS). ICP is rather a new method that is used in medical images to achieve rigid transformations. On the other hand, TPS is frequently used to perform elastic alignments. In our study, we have chosen these techniques to compare two similar but differently defined and expressed methods in order to align multimodal volumes. Before introducing the used methods how to transform medical images, it is indispensable to examine the transformation concepts and related processes through them.

2.1 Nature of the Transformations

In the most general case, two medical images may differ from one another by any amount of rotation about any axis, by any amount of translation in any direction and may differ in scale. In addition, straight lines in one image may map onto arbitrarily curved lines in the other image, and all of these features may vary locally throughout the volumetric extent of the images.

In image registration four types of transformations are commonly defined ;

1. **Rigid**; Rigid registration is the most commonly attempted method. Even in situations where a certain amount of elasticity is known to exist in the images objects (especially soft tissue) and/or in the imaging modality itself (as in MRI), rigid registration may be acceptable (or preferred, due to the complexities of nonrigid matching). Rigid transformations include rotation, translation, and reflection, but do not include scaling. Parallel straight lines map onto parallel straight lines.

2. **Affine**; Affine transformations include all the rigid transformations plus both uniform and nonuniform scaling and shearing. Straight lines map to straight lines, but parallelism may not always be preserved. Affine transformations are composed of a linear transformation of the same dimension as the geometry, plus a translation.

3. **Projective**, Projective transformations are linear transformations in a dimensional space higher than the geometry. They have particular application in cases where a 2-D projection is to be registered to a 3-D volume, but since projective transformation includes affine transformation, the framework may be used in other situations to provide a model of more difficult deformations. Straight lines map to straight lines but parallelism may not be preserved.

4. **Curved - Elastic**; Curved transformations map straight lines to arbitrary analytic curves. This is the most general case of transformations and can be seen to include projective transformations. *Polynomials*, *B-Splines*, and *Thin-Plate splines* are commonly used for curve projections. These choices illustrate the practical need to easily calculate curve parameters to fit a measured curve and specify the curve with a limited number of parameters, while still effecting smooth results.

A rigid or affine 3-D transformations can be described using a single constant matrix equation: $y_i = a_{ij}x_j$, where x and y are the old and new coordinate vectors respectively. In the rigid case, this equation is constrained as;

$$\begin{pmatrix} y_1 \\ y_2 \\ y_3 \\ 1 \end{pmatrix} = \begin{pmatrix} & \mathbf{R} & & \mathbf{T} \\ & & & \\ 0 & 0 & 0 & 1 \end{pmatrix} \begin{pmatrix} x_1 \\ x_2 \\ x_3 \\ 1 \end{pmatrix} \tag{2.1}$$

where T is an arbitrary translation vector, and R is a 3×3 rotation matrix defined by

$$R_{il} = R_{ij}^{(1)} R_{jk}^{(2)} R_{kl}^{(3)} \tag{2.2}$$

$$R^{(1)} = \begin{pmatrix} 1 & 0 & 0 \\ 0 & \cos\alpha_1 & -\sin\alpha_1 \\ 0 & \sin\alpha_1 & \cos\alpha_1 \end{pmatrix} \tag{2.3}$$

$$R^{(2)} = \begin{pmatrix} \cos\alpha_2 & 0 & \sin\alpha_2 \\ 0 & 1 & 0 \\ -\sin\alpha_2 & 0 & \cos\alpha_2 \end{pmatrix} \tag{2.4}$$

$$R^{(3)} = \begin{pmatrix} \cos\alpha_3 & -\sin\alpha_3 & 0 \\ \sin\alpha_3 & \cos\alpha_3 & 0 \\ 0 & 0 & 1 \end{pmatrix} \tag{2.5}$$

$R^{(i)}$ rotates the image around axis i by an angle α_i. In the affine case, R is unrestricted. In the projective case, we can only use a constant matrix representation if we are employing homogenous coordinates: $y_i = u_i/u_4$, $u_i = a_{ij}x_j$, where a is an arbitrary 4×4 constant matrix.

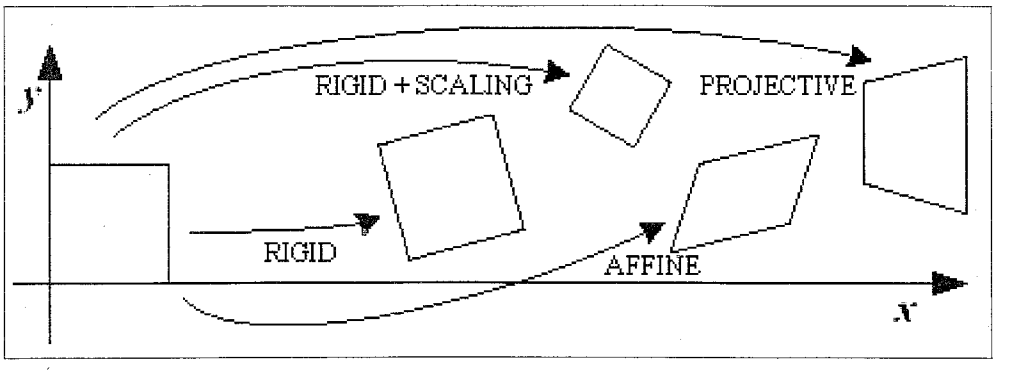

Figure 2.1 Basic Transformations.

Curved transformations cannot in general be represented using constant matrices. Most applications represent curved transformations in terms of a local vector displacement (disparity) field: $y_i = x_i + t_i(x)$, or as polynomial transformations in terms of the old coordinates.

2.2 Surface Based Registration

The 3-D boundary surface of an anatomic object or structure is an intuitive and easily characterized geometrical feature that can be sued for medical image registration. Surface based image registration methods involve determining corresponding surfaces in different images (and/or physical space) and computing the transformation that best aligns these surfaces.

The skin boundary surface (air-skin interface) and the outer cranial surface are obvious choices that have frequently been used for both image-to-image(e.g, CT-MR, T1-PD, T2-PD) and image-to-physical registration of head images. The surface representation can be simply a point set (i.e., a collection of points on the surface), a faceted surface (e.g., triangle set), an implicit surface, or a parametric surface (e.g., B-spline surface). **Extraction of a surface** such as the skin or bone is relatively easy and fairly automatic for head CT and MR images. **Extraction of many soft tissue boundary surfaces** is generally more difficult and less automatic. Utilization of sophisticated approaches is crucial depending on the physiology of soft tissues.

Image segmentation algorithms can generate 2-D contours in similar image slices that are linked together to form a 3-D surface, or they can generate 3-D surfaces directly from the image volume. In physical space, skin surface points can be easily determined using laser range finders; stereo video systems; and articulated mechanical, magnetic, active and passive optical, and ultrasonic 3-D localizers. Bone surface points can be found using tracked A-mode and B-mode ultrasound probes. The computer vision sensors, 3-D localizers, and tracked A-mode ultrasound probes produce surface point sets. Tracked B-mode probes produce a set of 2-D images from which bone surface points need to be segmented.

Surfaces can provide basic features for both rigid-body and nonrigid registration. A central and difficult question that must be addressed by any nonrigid surface based registration algorithm is how deformation of the contents of an object is related

to deformation of the surface of the object. Most of the surface based registration algorithms that have been reported are concerned with rigid-body transformation, occasionally with isotropic or non-isotropic scaling. Thus, **most of the cortical registration** researches are based on *rigid body* transformation due to anatomical and physiological properties. On the other hand, in **abdominal registrations** an *elastic surface based* transformation is preferred.

2.3 Landmark or Intensity Based Registration

According to the surface based methods, current registration techniques can be clustered into two categories : landmark based or intensity based. Each category can be subclassified according to the methodology followed by the algorithms. Generally the subcategories are clustered regarding of the linearity and the nonlinearity.

The landmark based approach generally involves extracting corresponding or equivalent landmarks from the image to be registered and determining the transformation parameters that relate to those corresponding landmarks. On the other hand, the intensity based approach eliminates the landmark extraction step by creating a cost function from the voxel intensity space directly, and optimizing this function among different transformations parameters. Fischer et al. [14] introduced a theoretical approach for the combination of intensity and landmark based methods.

After the determination of corresponding surfaces, in our study we will consider two different landmark based approaches; Iterative Closest Point (ICP) algorithm and Thin Plate Splines (TPS).

2.3.1 Iterative Closest Point (ICP) Algorithm

The Iterative Closest Point Algorithm (ICP) is a method for bringing into registration two partially overlapping but slightly misaligned range images. ICP has proven to be very useful in the processing of range data, and a number of variations on the basic method have been proposed. These include alternate transformation calculations, the use of intensity information and curvature, and outlier selection filters.

At each iteration, corresponding points between two images are determined by a Nearest Neighbor (*NN*) method. Determining these correspondences accounts for the majority of the runtime expense of ICP. In their original paper, Besl et al. [15] suggested the use of the K-d tree method. They also noted that other Nearest Neighbor methods may be suitable and there have been some prior explorations into the use of alternatives. Other researchers tried to develop advanced techniques based on ICP in other to obtain more accurate results and ensure efficient linear operations. Greenspan et al. [16] explored the use of an Approximate Nearest Neighbor method for improving the runtime efficiency of ICP. Gelfand et al. [17] proposed a better point selection method to eliminate the major drawback of ICP convergence. The uncertainty of the object pose is clearly identified and the point pairs of ICP are well estimated in the same article.

Briefly, this iterative method can handle rigid transformations, that are transformations consisting of rotations and translations. A priori knowledge of the correspondence between points is not necessary. In our work, we attempted to register two different points sets retrieved form different imaging sensors. Therefore, a multimodal registration using points located on the surface of the image is done.

In the following part, we will introduce the methodology of ICP registration for two different point sets; *template* and *target*.

Let N_p and N_x be the number of points in sets P, X, respectively:

$$P = \{p_i\} \qquad i = 1, \cdots, N_p \tag{2.6}$$

$$X = \{x_i\} \qquad i = 1, \cdots, N_x \tag{2.7}$$

where in our case p_i and x_i are 3-D vectors (voxel coordinates) :

$$x_i = \begin{bmatrix} x_i & y_i & z_i \end{bmatrix} \tag{2.8}$$

The ICP algorithm evaluates the correspondence between the two point sets, estimates the optimum registration vector, that is the set of translation and rotation parameters that lead to the optimum registration of the two sets and then applies this transformation to one of the sets. This process is applied repeatedly until a certain dissimilarity measure becomes smaller than a certain value.

The ICP algorithm registers sets P, X by evaluating for each point p_i in P its corresponding point in X, i.e., the point in X with the minimum distance. This operation is called *evaluation of the distance between a point and a data set* and is denoted by $d(p_i, X)$:

$$d(p_i, X) = \min_{j \in \{1, \cdots, N_x\}} d(p_i, x_j) \tag{2.9}$$

where $d(p_i, x_j)$ is the Euclidean distance of the two points. This process is repeated for all points in P so that, for each point p_i, the closest point x_j in X, denoted by y_i, is found. This results in the construction of the set Y of closest points, a process that is denoted by the operator C:

$$Y = C(P, X) \tag{2.10}$$

where $Ny = Np$.

Having evaluated the correspondence between the two point sets, the ICP al-

gorithm proceeds to the evaluation of the translation and rotation parameters that lead to the optimum registration of the two sets Y, X. This is done using *quaternions*. *Quaternions* are a means of representing 3-D rotations. A unit quaternion is a four-dimensional vector $q_R = \begin{bmatrix} q_0 & q_1 & q_2 & q_3 \end{bmatrix}^T$ such that $q_0 \geq 0$ and $q_0^2 + q_1^2 + q_2^2 + q_3^2 = 1$. Rotation by an angle θ around a unit vector $[x_1\ x_2\ x_3]^T$ can be represented by the following quaternion:

$$q_R = \begin{bmatrix} \cos\frac{\theta}{2} & x_1 \sin\frac{\theta}{2} & x_2 \sin\frac{\theta}{2} & x_3 \sin\frac{\theta}{2} \end{bmatrix}^T \tag{2.11}$$

The rotation matrix $\mathbf{R}$ that corresponds to a certain quaternion is the following:

$$R(q_R) = \begin{bmatrix} q_0^2 + q_1^2 - q_2^2 - q_3^2 & 2(q_1 q_2 - q_0 q_3) & 2(q_1 q_3 + q_0 q_2) \\ 2(q_1 q_2 + q_0 q_3) & q_0^2 + q_2^2 - q_1^2 - q_3^2 & 2(q_2 q_3 - q_0 q_1) \\ 2(q_1 q_3 - q_0 q_2) & 2(q_2 q_3 + q_0 q_1) & q_0^2 + q_3^2 - q_1^2 - q_2^2 \end{bmatrix} \tag{2.12}$$

A 3-D translation can be defined by the vector $q_T = \begin{bmatrix} q_4 & q_5 & q_6 \end{bmatrix}^T$. The two vectors can be combined in a single *registration vector.*

$$q = \begin{bmatrix} q_R \\ q_T \end{bmatrix} = \begin{bmatrix} q_0 & q_1 & q_2 & q_3 & q_4 & q_5 & q_6 \end{bmatrix}^T \tag{2.13}$$

The optimal registration vector is the one that minimizes the mean square error function:

$$f(q) = \frac{1}{N_p} \sum_{i=1}^{N_p} \| y_i - R(q_R) p_i - q_T \|^2 \tag{2.14}$$

For the evaluation of the optimum q_R, q_T, we first evaluate the centers of the mass μ_P, μ_y of point sets P, Y, respectively:

$$\mu_P = \frac{1}{N_p} \sum_{i=1}^{N_p} p_i \tag{2.15}$$

$$\mu_Y = \frac{1}{N_y} \sum_{i=1}^{N_y} y_i \tag{2.16}$$

The cross-covariance matrix of P, Y is evaluated next:

$$\sum_{p,y} = \frac{1}{N_p} \sum_{i=1}^{N_P} \left[(p_i - \mu_p)(y_i - \mu_y)^T \right] \tag{2.17}$$

Then the column vector Δ is formed :

$$\Delta = \begin{bmatrix} A_{23} & A_{31} & A_{12} \end{bmatrix}^T \tag{2.18}$$

where A_ij are the i, j elements of the matrix $(\sum_{py} - \sum_{py}^T)$. Finally, a 4×4 matrix of the following form is generated:

$$Q(\sum_{py}) = \begin{bmatrix} tr(\sum_{py}) & \Delta^T \\ \Delta & \sum_{py} + \sum_{py}^T - tr(\sum_{py}) I_3 \end{bmatrix} \tag{2.19}$$

where $tr()$ is the trace of a matrix, which is the sum of its diagonal elements, and I_3 is the 3×3 identity matrix. The unit eigenvector that corresponds to the maximum eigenvalue of $Q(\sum_{py})$ is the optimal rotation quaternion q_R. The optimal translation vector is chosen to be

$$q_T = \mu_y - R(q_R)\mu_p \tag{2.20}$$

After the initialization of mathematical foundations as described above, we can introduce the ICP implementation as it follows:

The parameters evaluated in the previous step are then used to translate and rotate the data set P:

$$P = q(P) \tag{2.21}$$

where $q(P)$ denotes transformation of set P using the registration vector q.

For the first iteration of the algorithm (iteration steps $k = 0$), the data set is initialized using the initial point set $P_0 = P$, whereas the registration vector q is initialized as follows:

$$q_0 = \begin{bmatrix} 1 & 0 & 0 & 0 & 0 & 0 & 0 \end{bmatrix} \tag{2.22}$$

Then the algorithm proceeds as follows :

1. The closest points are computed using Eq. 2.10.
2. The optimal registration vector q_k is evaluated as described above.
3. The data set P is translated and rotated using the registration vector evaluated in the previous step: $P_k + 1 = q_k(P_k)$
4. If the mean squared error (Eq. 2.14) is below a certain threshold then the algorithm stops. Otherwise, steps 1 through 4 are prepared using $P_k + 1$.

Table 2.1
Pseudocode of Iterative Closest Point Algorithm.

ICP (Target, Template);
begin
$E' \leftarrow +\infty$;
$(Rotation, Translation) \leftarrow Initialize\_Registration(Template, Target)$;
repeat
$E \leftarrow E'$;
$Registered\_Template \leftarrow Apply\_Registration(Template, Rotation, Translation)$;
$Pairs \leftarrow Closest\_Pairs(Registered - Template, Target)$;
$(Rotation, Translation, E') \leftarrow Update\_Registration(Template, Target, Pairs, Rotation, Translation)$;
$until|E' - E| < \tau$;
return (Rotation, Translation);
end

As the ICP procedure is summarized in Table 2.1, we notice that the auxiliary function *Initialize_Registration* uses some global registration method based on

moments, for example, to compute a rough initial estimate of the rigid transformation mapping the template onto the target. The function *Closest_Pairs* returns the indexes (i, j) of the points in the registered scene and the target such that point number j is the closest to the point number i. The function *Update_Registration* estimates the rigid transformation between selected pairs of points in the template and the target, and the function *Apply_Registration* applies a rigid transformation to all points in the target.

As a result of the recent descriptions it is clear that ICP is a representation-independent method for the accurate and computationally efficient registration of 3-D shapes including free-form curves and surfaces.

Concisely, it is notable that ICP algorithm always converges monotonically to the nearest local minimum of the nearest local minimum of a mean-square distance metric, and experience shows that the rate of convergence is rapid during the first few iterations. At a glance the shape registration algorithm can be used with the following representations of geometric data;

1. Point sets.
2. Line segment sets (polylines).
3. Implicit curves $\vec{g}(x, y, z) = 0$.
4. Parametric curves: $(x(u), y(u), z(u))$.
5. Triangle sets (faceted surfaces).
6. Implicit surfaces: $g(x, y, z) = 0$.
7. Parametric surfaces: $x(u, v), y(u, v), z(u, v)$.

Most frequently, image registration techniques based on linear transformations have been applied to the head. It is obvious that using a linear approach would give better results in the head which is a more rigid structure than the chest or abdomen.

Furthermore, since ICP is a pseudo-linear local search algorithm, it suffers from many problems commonly associated with local searches, such as slow convergence (due to shallow error landscapes) and the tendency to fall into local minima. The point selection strategy and the choice of error metric to be minimized play a large role in both the rate of convergence and the accuracy of the resulting pose.

Poor alignment between a pair of meshes can come from several sources. Noise in the input data can cause ICP to converge to a local minimum. The frequency of local minima in the error landscape depends on the input geometry and on the minimized distance metric.

The extension of ICP to non-rigid methods are thought as a new approach to overcome these limitations. Feldmar et al. [18] introduced an intensity based method mixed up with ICP. In the same article it is shown that matchings on heart and brain tissues present good alignments.

2.3.2 Elastic Registration

In neurosurgery and radiotherapy it is important to either register images from different modalities, e.g. CT and MR images, or to match images to atlas representations. If only rigid transformations were applied, then the accuracy of the resulting match often is not satisfactory with respect to clinical requirements. In general, non-rigid transformations are required to cope with the variations between the data sets. A special class of general nonrigid transformations are elastic transformations which allow for local adaptivity and are constrained to some kind of continuity or smoothness.

This contribution is concerned with elastic registration of medical image data based on a set of corresponding anatomical landmarks. Such a feature-based approach comprises three steps:

1. Extraction of landmarks in the different data sets.
2. Establishing the correspondence between the landmarks.
3. Computing the transformation between the data sets using the information from (1) and (2).

Among the different types of landmarks (points, lines, surfaces, and volumes) in our thesis we consider point landmarks for 3D registration.

2.3.3 Clinical Applications for Elastic Registration

Although elastic matching is not routinely used in clinical practice yet, there are several applications in which elastic matching is believed to improve current therapeutical procedures.

2.3.3.1 Image-Atlas Matching. One possible application of elastic alignment is trajectory planning for neurosurgical intervention. Pain treatment as well as epilepsy treatment sometimes require to localize a functionally important region not visible in the available image data. There are instructions available in the literature how to construct the position of such a region given landmarks which can be identified in CT or MR images. Hence, it is useful to superimpose an atlas with a medical image.

Due to the individual variability of anatomical structures, rigid registration is generally not sufficient and elastic matching should be applied. The approach introduced by Szeliski et al. [19] could be applied directly to brain surfaces for image-atlas matching. The spline utilization would perform good alignments through inward and outward surfaces depending on the segmentation algorithms in preprocessing treatment. Hamadeh et al. [20] extended the same method and applied it directly for computer integrated surgery. It is shown on real examples that a methodology based

on surface distance minimization between anatomical reference structures can be used efficiently with many different types of data.

2.3.3.2 CT-MR Matching. Another application for elastic alignment is the registration of CT and MR images for the purpose of radiotherapy planning. Additionally, a template atlas can be superimposed on the MR image to indicate, for example, organs at risk. This superposition result is then overlayed on the CT image prior to dose calculation and isodose visualization on the MR image.

By the way, the article of Maintz et al. [21] is a suitable example for MR-CT elastic alignment. The utilization of edge and ridge operators give accurate 3D matching results and local distortions or warpings are reduced .

On the one hand, scanner-induced distortions have to be coped with which are caused by, e.g., inhomogeneities of the main magnetic field, imperfect slice or volume selection pulses, nonlinearities of the magnetic field gradients, and eddy currents. On the other hand, there are geometrical distortions in MR images that are induced by the patient and cannot be removed by calibration. Parameters such as susceptibility variations, chemical shift for non-water protons and flow-induced distortions for vessels are very important. While the susceptibility difference of tissue and air is approximately 10^{-5}. Consequently, due to the scanner -as well as the patient- induced distortions of the MR image, CT and MR images cannot be satisfactorily registered using a rigid transformation.

2.3.4 Thin-Plate Splines (TPS)

The most widely applied method for landmark oriented elastic image registration is based on thin-plate splines. Even if the methodology has been introduced in 1976 by Duchon, this approach has been well presented in **medical** image analysis by Bookstein [22] who applied first this scheme to 3D medical images. Thin-plate splines have a

physical motivation, are mathematically well-founded, and are moreover computationally efficient. Alternative splines based on the Navier equation has been also utilized with medical data sets. Extensions of point-based elastic schemes which allow to include additional attributes at landmarks have been proposed by Bookstein and Green. The combination of thin-plate splines with mutual information as similarity measure for the purpose of refining initially coarsely specified landmarks has been studied by Meyer. Also recently, Christensen [23] introduced a hierarchical approach to image registration combining a landmark-based scheme with an intensity-based scheme using a fluid model. The landmark scheme is based on the linear elasticity operator and the applied splines differ from thin-plate splines. Another intensity-based approach which tries to integrate landmark errors has been developed by Gee. However, this approach is not based on analytic solution of the underlying functions but solves it numerically by applying the finite element method, which is computationally much more expensive.

In all of these approaches, the interpolation case has been treated. This means that corresponding landmarks are forced to match exactly and thus it is implicitly assumed that the landmark positions are known exactly. This assumption, however, is unrealistic since landmark extraction is generally prone to error.

Recently Lewis et al. [24] emphasized the importance of landmark selection for TPS. They showed the quality of the registration with respect to user's choice of landmark placement. In the same study, ambiguous landmarks are removed. Only the landmarks along the contours that depict image boundaries are conserved. Hence, the thin plate spline energy is minimized and the undesired degree of freedom are removed. In our study, we followed the same rule and tried to eliminate undesired landmarks by selecting them through the skull surface.

The term spline originally refers to the use of long flexible strips of wood or metal to model the surfaces of ships and planes. These splines were bent by attaching different weights along its length. A very similar concept can be used to model spatial transformations. For example, a 2D transformation can be represented by two separate surfaces whose height above the plane corresponds to the displacement in the horizontal

or vertical direction.

2.3.4.1 Control Points in TPS. Many registration techniques using splines are based on the assumption that a set of corresponding points or landmarks can be identified in the source and target images. These corresponding points are often referred to as *control points*. At these control points, spline-based transformations either interpolate or approximate the displacements which are necessary to map the location of the control point in the target image into its corresponding counterpart in the source image. Between control points, they provide a smoothly varying displacement field.

There are a number of different ways of how the control points can be determined. For example, anatomical or geometrical landmarks which can be identified in both images can be used to define a spline-based mapping function which maps the spatial position of landmarks in the source image into their corresponding position in the target image.

About the landmark determination procedure, there are several procedures studied in different papers according to the application area and method, especially in brain and cortical surface extractions. Rohr et al. [25, 26, 27, 28, 29, 30] proposed a semi automatic landmark localization by introducing a ROI selection in 2D. In our simulation study we followed a similar approach. Elsen et al. [31] offered also a near automatic marker detection method for MR-CT registrations. The latter has proposed also a new approach for marker detection accuracy. It is also stated that the algorithm can be extended to the detection of marker tubes in PET and SPECT images.

Either intrinsic or extrinsic, TPS requires an extra step for the determination of control or reference points. The energy minimization between considered slices/volumes is achieved depending on their localization.

2.3.4.2 Mathematical Foundations. Thin-plate splines are part of a family of splines which are based on radial basis functions. They have been formulated for the surface interpolation of scattered data. Radial basis function splines can be defined as a linear combination of n radial basis functions $\theta(s)$:

$$\phi(x,y,z) = a + b_x x + b_y y + b_z z + \sum_{k=1}^{n} w_k \theta(|\psi_j - (x,y,z)|) \tag{2.23}$$

or

$$\phi(x,y,z) = a + b_x x + b_y y + b_z z + \sum_{k=1}^{n} w_k g(\sqrt{(x-x_k)^2 + (y-y_k)^2 + (z-z_k)^2}) \tag{2.24}$$

In our thesis, we considered two different forms of radial basis functions for 2D and 3D image registrations. However in our simulation study we used the 3D case. They are defined as it follows;

$$\theta(r) = \begin{cases} |r|^2 \log(|r|) & \text{in 2D,} \\ |r| & \text{in 3D.} \end{cases} \tag{2.25}$$

Thus, we denote from Eq. 2.23 and Eq. 2.24 that

$$\begin{gathered} U(p - p_k) = \theta(|\psi_j - (x,y,z)|) \\ U(p - p_k) \approx g(\sqrt{(x-x_k)^2 + (y-y_k)^2 + (z-z_k)^2}) \end{gathered} \tag{2.26}$$

Let $K_i = Q_i - P_i$ $i \in \{1, \cdots, n\}$ where Q and P are template and target landmarks and n is the total number of landmarks. In our measurements, when we registered multimodal head images, we have chosen this n between 8 and 20. K_i depicts the displacement between corresponding landmarks. Therefore, we can rewrite a set of

equations in order to express the global formulation:

$$\begin{bmatrix} K_1 \\ K_2 \\ \vdots \\ K_N \end{bmatrix} = \begin{bmatrix} \sum_{k=1}^{n} w_k U(p_1 - p_k) + a + b_x q_{1x} + b_y q_{1y} + b_z q_{1z} \\ \sum_{k=1}^{n} w_k U(p_2 - p_k) + a + b_x q_{2x} + b_y q_{2y} + b_z q_{2z} \\ \vdots \\ \sum_{k=1}^{n} w_k U(p_n - p_k) + a + b_x q_{nx} + b_y q_{ny} + b_z q_{nz} \end{bmatrix} \tag{2.27}$$

Defining the transformation as three separate thin-plate spline functions $T = (t_1, t_2, t_3)^T$ yields a mapping between images in which the coefficients as expressed in Eq. 2.23 and Eq. 2.24. a, b_x, b_y and b_z characterize the affine part of the spline-based transformation while the coefficients, w characterize the non-affine part of the transformation.

Modeling deformations using thin-plate splines has a number of advantages. For example, they can be used to incorporate additional constraints such as rigid bodies or directional constraints into the transformation model. They can be extended to approximating splines where the degree of approximation at the landmark depends on the confidence of the landmark localization.

The variation function of our thin-plate spline is defined in Eq. 2.24. By the way, it can also be redefined in a more compact matrix form

$$\phi(\vec{v}) = a + \vec{b}^T \vec{v} + W^T \vec{g}(\vec{v}) \tag{2.28}$$

where

$$\vec{v} = \begin{bmatrix} x \\ y \\ z \end{bmatrix} \quad \vec{b} = \begin{bmatrix} b_x \\ b_y \\ b_z \end{bmatrix} \quad W = \begin{bmatrix} w_1 \\ w_2 \\ w_3 \end{bmatrix} \tag{2.29}$$

and

$$\vec{g}(x,y,z) = \begin{bmatrix} \sqrt{(x-x_1)^2+(y-y_1)^2+(z-z_1)^2} \\ \sqrt{(x-x_2)^2+(y-y_2)^2+(z-z_2)^2} \\ \vdots \\ \sqrt{(x-x_n)^2+(y-y_n)^2+(z-z_n)^2} \end{bmatrix} \tag{2.30}$$

In addition, the following constraints are imposed in order to allow minimal energy.

$$\sum w_k = \sum w_k x_k = \sum w_k y_k = \sum w_k z_k \ . \tag{2.31}$$

It is clear from Eq. 2.24 and 2.28 that the thin-plate spline $\phi(x,y,z)$ involves three main parts: (i) a constant term a_0; (ii) the internal product between the coefficient vector $\vec{b}$ and $\vec{v}$, i.e., $\vec{b}^T\vec{v}$; and (iii) a linear combination of basic functions $g(x,y,z)$, centered at each of the n points $\vec{p}_k = (x_k, y_k, z_k)$. Each thin-plate fit to a set of control points is guaranteed to have *minimal bending energy* E, which is defined for 2D as;

$$E = \sum_{k=1}^{2} \int_{x=-\infty}^{\infty} \int_{y=-\infty}^{\infty} [(\frac{\partial^2 \phi_k}{\partial x^2})^2 + 2(\frac{\partial^2 \phi_k}{\partial x \partial y}) + (\frac{\partial^2 \phi_k}{\partial y^2})^2] dx dy \ . \tag{2.32}$$

Concisely, it is showed that we use this bending energy function to calculate the minimum cost value in order to find the minimum distance between the control points. Therefore, let's explain how to find the feasible solutions with respect to the expressions introduced until here.

Firstly, we have to build up a matrix that concerns the Euclidean distance between each set of control points. It is clear that all of the equations are for 3D registration. Hence, the $n \times n$ matrix T including the values of the basic function $g(x,y,z)$ evaluated at each of the distances defined between each pair of control points is:

$$T = [g(\rho_{i,j})]_{nxn} = \begin{bmatrix} 0 & g(\rho_{1,2}) & \cdots & g(\rho_{1,n-1}) & g(\rho_{1,n}) \\ g(\rho_{2,1}) & \ddots & \cdots & g(\rho_{2,n-1}) & g(\rho_{2,n}) \\ \vdots & \vdots & 0 & \vdots & \vdots \\ g(\rho_{n-1,1}) & g(\rho_{n-1,2}) & \cdots & \ddots & g(\rho_{n-1,n}) \\ g(\rho_{n,1}) & g(\rho_{n,2}) & \cdots & g(\rho_{n,n-1}) & 0 \end{bmatrix} \tag{2.33}$$

where

$$\rho_{i,j} = \sqrt{(x - x_k)^2 + (y - y_k)^2 + (z - z_k)^2} \ . \tag{2.34}$$

Secondly, the $n \times 4$ matrix S_e containing the x, y and z coordinates of the control points, plus an initial column of ones is:

$$S_e = \begin{bmatrix} 1 & x_1 & y_1 & z_1 \\ 1 & x_2 & y_2 & z_2 \\ \vdots & \vdots & \vdots & \vdots \\ 1 & x_n & y_n & z_n \end{bmatrix} \tag{2.35}$$

Thirdly, the $(n+4) \times (n+4)$ matrix M obtained by composing the matrices T and S_e is formed as follows:

$$M = \begin{bmatrix} T & S_e \\ S_e^T & 0 \end{bmatrix} \tag{2.36}$$

Finally, we should combine all of these equations to solve the system and obtain the minimum energy. For the sake of a feasible solution, we construct a $n+4 \times 1$ matrix C containing all the sought coefficients involved in Equations (2.23) and (2.27)

$$C = (w_1, w_2, \cdots, w_N, a, b_x, b_y, b_z)^T \ . \tag{2.37}$$

Now, we rewrite the equation that we introduced in Eq. 2.27.

$$K = (K_1, K_2, \cdots, K_N, 0, 0, 0, 0)^T \quad . \tag{2.38}$$

Now, the sought coefficients required to interpolate through the n control points can be easily obtained by solving the following matrix equation, provided the matrix M is not singular:

$$K = MC \Rightarrow C = M^{-1}K \quad . \tag{2.39}$$

Finally, the bending energy can be immediately obtained as;

$$E = W^T T W \tag{2.40}$$

where W is the $n \times 1$ vector containing the n first rows of C.

2.4 Matching Performance and Error Analysis

Generally three types of cost functions or measures of goodness of matching have been developed in image registration. They are based on;

1. Corresponding points.
2. Corresponding surfaces (both corresponding points and surfaces).
3. Corresponding image features (e.g.intensities).

2.4.1 Corresponding Points

The most straightforward registration error metric is the mean Euclidean distance between corresponding points in both images. The mean square error is also used,

primarily to avoid the computational expense of taking a square root. Either function can be expected to exhibit a global minimum at the point of perfect registration, and to increase monotonically with increased misregistration.

The corresponding points may be determined either by attaching extrinsic fiducial markers rigidly to patient bony structures, or by expert identification of intrinsic anatomic landmarks. In both cases, analytic solution of a minimal set is generally confounded by errors in landmark or marker localization, either by human or computer. In some cases, an over specified set of points (more than 30-40 points) is used. The contribution of the various points may be weighted by a factor related to the certainty of the landmark identification or by the distance of the landmark from the image center. These modifications seek to lower the influence of ambiguous landmarks and lend greater weight to points that are more severely displaced by rotation.

2.4.2 Corresponding Surfaces

Corresponding image surfaces have been widely used for intra- and intermodality registration. The corresponding surfaces may be simple isosurfaces or carefully hand-segmented contours. There is also application of surface-based registration in intraoperative registration of image data to real-world patient coordinates. The surfaces selected must generally correspond, and rigid structures are preferable to soft tissues as surface features.

The most striking differences between surface-based metrics and landmark/fiducial-based metrics is the greater number of coordinate points involved in surface registration, and the complete lack of correspondence information. It is explicitly known which landmark or fiducial in one image corresponds to which feature in the other image, but there are only a few landmarks.

Mean squared error is a common way to express the difference between two dependent curves or surfaces, and use of this measure can be effective by recasting the

measurement in a coordinate system where the surfaces are dependent. For example, the surface of a brain is clearly not a dependent surface of any pair of Cartesian axes, but in a spherical coordinate system with the origin at the centroid of the brain, the brain surface is (discounting sulci) a radial function of alpha and theta. This technique has been used to match MR head images with corresponding PET images measuring mean squared error in this way.

Other metrics use of the concept of *Chamfer Distance*. Chamfer distance is the shortest discrete line from a specific point on one surface to any point on the other surface. The advantage of chamfer distance is that it is a "field" that can be calculated for all voxel coordinates in one image relative to one surface alone. Briefly, this method is defined with a cost function minimization. It assumes that the best registration is achieved at the point where the cost function reaches the global minimum. This assumption is true only if:

1. There is only one global minimum point in the cost function.
2. The match surface is not severely distorted relative to the base surface.
3. Every sampled match surface point has a corresponding point existing on the base surface.

First assumption is satisfied for most medical images that have no rotational symmetry, that is, there exists only one true matching position. The second assumption must be satisfied in order for the assumption of rigid body to be true. If it is not satisfied, then a more complicated alignment (generally an elastic approach) should be used. The last assumption will be satisfied if the images are acquired so that the base/template volume contains the match/target volume, and if there is no noise or distortion to add an extra component to match volume.

2.4.3 Corresponding Image Features

For intramodality registration, the mean squared error (MSE) between corresponding image voxels should have the required minimum at the point of proper registration. This method is usually used in the intramodal case, but is in fact easily confounded by incompletely corresponding image volumes and treatment influenced anatomic changes. One approach to practical intra- and intermodal voxel similarity-based registration is based on minimizing the normalized standard deviation of the gray values of voxels in one image that correspond to voxels of a single gray value in the other.

A number entropy-based measures have been suggested in which the joint entropy among images is minimized, or conversely the mutual information among the images is maximized.

As a summary, in both images extrinsic or intrinsic markers are identified. The exact correspondence between markers is known, so registration may be established by minimizing the average Euclidean distance between corresponding markers. The efficiency of registration is measured by means of this final results according to the formulation of joint entropy if we consider an intensity-based approach. Otherwise, a MSE or RMS analysis would be introduced in morphometric alignment.

2.4.4 Evaluating and Validating Image Registration

The accuracy of a particular coregistration transform matrix, and consequently the performance of a registration algorithm becomes more difficult to assess as the test conditions approach the clinical setting. The basic performance of an algorithm can be extensively studied by translating and rotating a copy of an image volume by known amounts and then reregistering that copy to the original. The best-case accuracy of the algorithm can be assessed because the correct solution is exactly known. Additive

noise can be used to simulate real-world conditions more closely, gray scale remapping can be applied to simulate intermodal applications, and parts of the copy can be erased to simulate partially overlapping scans. Still, such contrived testing differs significantly from the task of registering two different real images of a patient independently acquired from different modalities.

To evaluate the registration of multimodality patient images in a clinical setting, the most common approach is to have an expert grade registrations for quality, or perform a manual registration to be taken as ground truth for the study. This has the advantage of relating the algorithm's performance directly to the currently used "gold standard", but there is seldom an available objective measure of the expert's performance. Using multiple experts significantly improves the repeatability of these studies, but residual error below the threshold of visual detection cannot be evaluated.

Anthropomorphic phantoms have proven valuable in validating multimodal registration algorithms. Phantom experiments have the advantage of a predictable, uniform construction of geometric features and are generally not subject to motion artifacts. This makes it possible to isolate different sources of error while evaluating registration results. Materials may be chosen to mimic tissue characteristics in multiple modalities, and the volume of phantom compartments can be measured or controlled to any desired accuracy. Although the orientation of the phantom images to each other may not be known, the position of rigidly attached markers provides for independent registration evaluation.

Patient motion artifacts can occur during conventional and spiral CT scans of any significant extent. Acquisitions requiring multiple breath-holds, and most gated imaging studies can be expected to exhibit a few section-to-section misalignments due to gross subject motion. Movement during MRI scans can also induce section-to-section misalignments, but also cause more subtle image quality degradation.

Furthermore, patient motion during multi-slice MR imaging can result in a variation in slice orientation relative to the patient across the scan. This is currently

an unsolved problem, and makes registration of such data sets very difficult. In the rigid body case, there is a different transformation needed for each slice (or in some MR images, groups of slices), and this transform is hard to find. Motion during MR imaging within the acquisition of a single slice or an entire 3D volume results in a different problem, namely *ghost artifacts*. This can result in one or more ghosts of the object appearing in the image along with the main image of the object. These ghosts normally have higher spatial frequency content than the main image, but there is a different registration transformation needed for each ghost.

Patient images with attached markers provide the most complete validation of rigid registration algorithms applied to real data. Generally, the markers are removed from the image data, and registration performed on the remaining image data. The determined registration matrix is applied to the original image, and the remaining displacement of marker centroids evaluates the registration quality. It is important that the markers be rigidly affixed, and must produce signal in all modalities under test. Interchangeable markers for different modalities can be used, but the mounting system must assure the physical alignment of centroids between different markers.

3. RESULTS

3.1 Initiation

In our study, we tried to register medical images retrieved from different imaging sensors. Briefly, we had 3 different types of imaging methods; MR, PET and SPECT modalities. By the way, MR images are subdivided into PD, T-1 and T-2 weighted classes. Therefore, we have taken into account 5 different modalities.

Even if MR based inter-registration is not common, we found that recently, in this area new projects using brain images have been studied in the analysis of Alzheimer's disease and Multiple Sclerosis [32].

We divided our simulation protocol into 3 sections; segmentation, volume reconstruction and registration. Hsu et al. [33] presented a similar approach in order to align brain images. The presented flow chart at the same article is subdivided into 3 sections like our study; edge detection (*image segmentation*), voxel reformation (*volume reconstruction*) and geometric transformation (*volume matching*). For TPS method as an intra-step the landmark determination could be noticed like a sub-segmentation step.

In our implementation a combination of point sets (for considered multimodal pairs) according to multimodal information is performed. Lemieux [34] applied a closer experiment protocol. Serial images of three patients are segmented in a similar way. Each patient had three scans which were registered first to second, second to third, third to first, and in the opposite sense.

In order to compare registration results we have taken into account two criteria; Mean of distance differences and Root Mean Square Analysis.

3.2 Image Segmentation and Volume Reconstruction

We considered two surface-based methods; ICP algorithm and TPS method. We note that all images are pixelwisely interpreted to visualize or to do some morphological operations when we register them with intensity-based methods. However, in our work we needed to obtain the skull surface information and the corresponding 3D positioning to set initial coordinates.

For this purpose, we applied a threshold value into 87 slices to relate them with binary images within all imaging modalities. Furthermore, we retrieved the skull surface information according to outer contours.

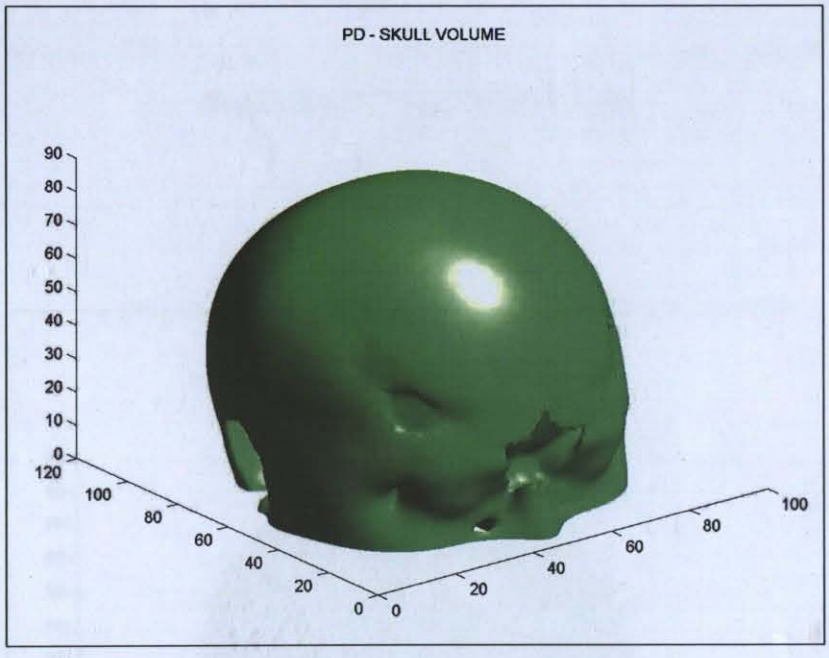

Figure 3.1 PD weighted MR Volume.

After the retrieval of surface information, we located these points into 3D cartesian coordinate system in order to build up a volume. Here, the surface information has been already calculated using polyline segmentation and the remnant was to place these polylines along z-axis with respect to volume resolution. In the Figures 3.1, 3.2, 3.3, 3.4 and 3.5 all points are positioned in 3-D Cartesian coordinate system and the surface which is meshed by these points are rendered. On the other hand, in 3.6, 3.7,

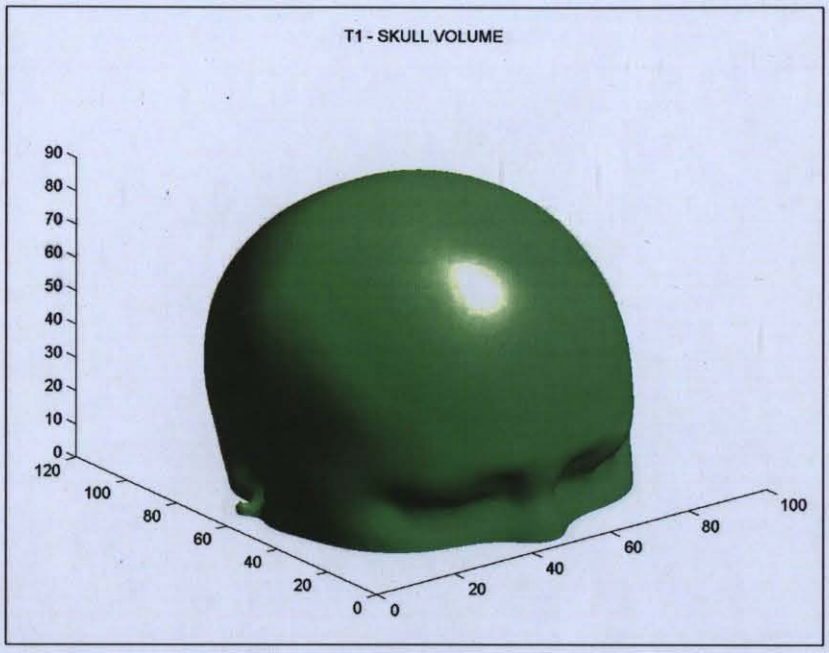

Figure 3.2 T1 weighted MR Volume.

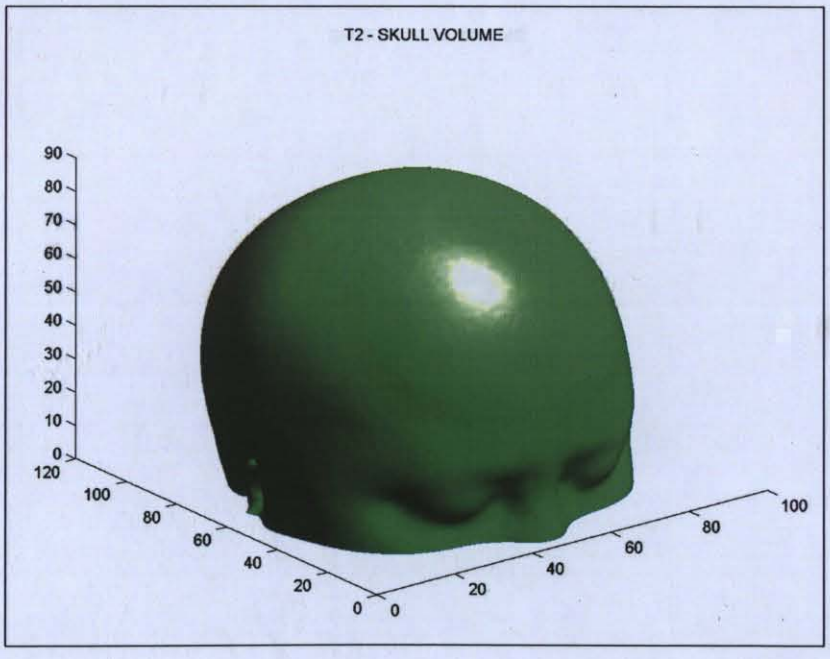

Figure 3.3 T2 weighted MR Volume.

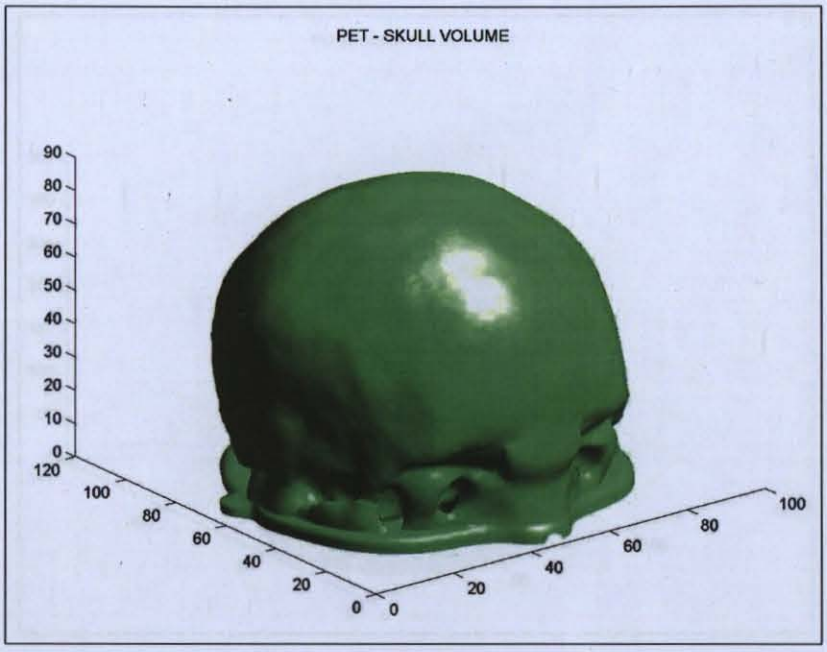

Figure 3.4 PET Volume.

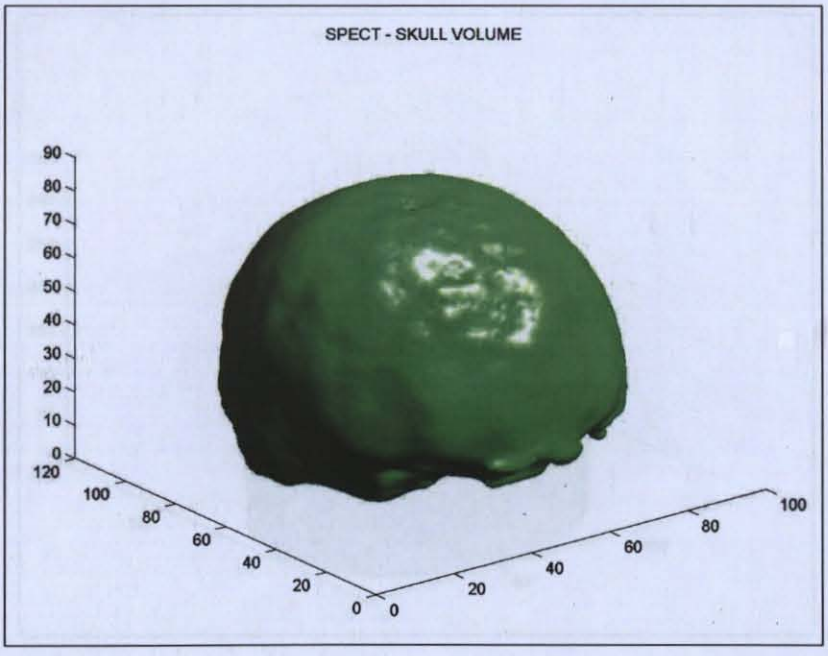

Figure 3.5 SPECT Volume.

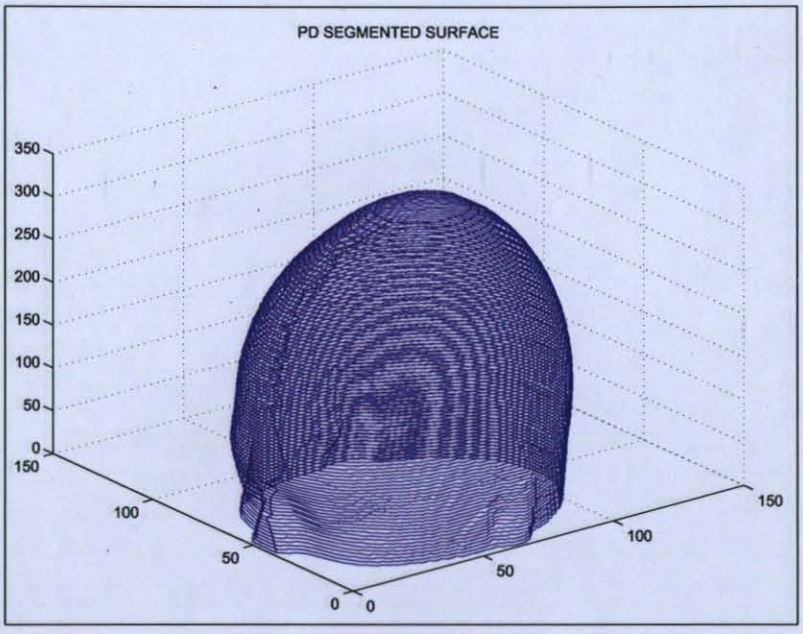

Figure 3.6 Segmented PD Volume.

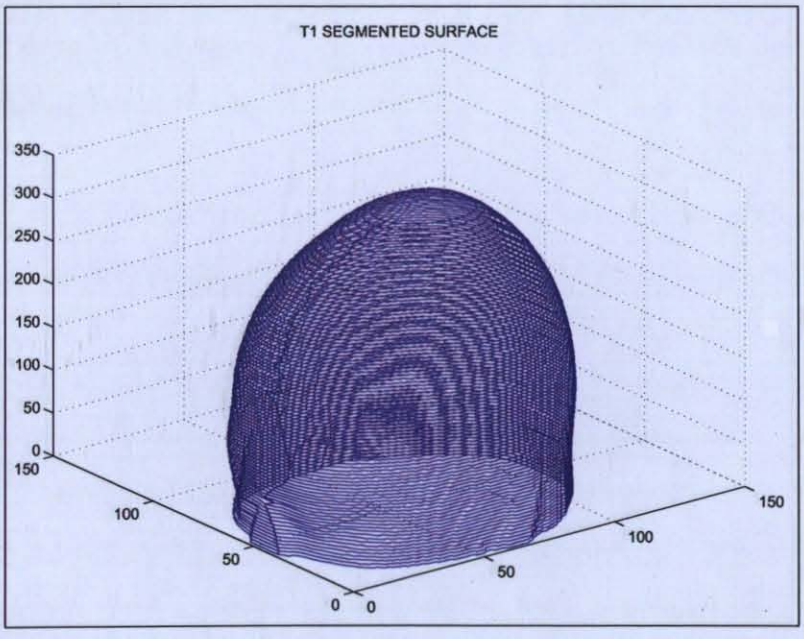

Figure 3.7 Segmented T1 Volume.

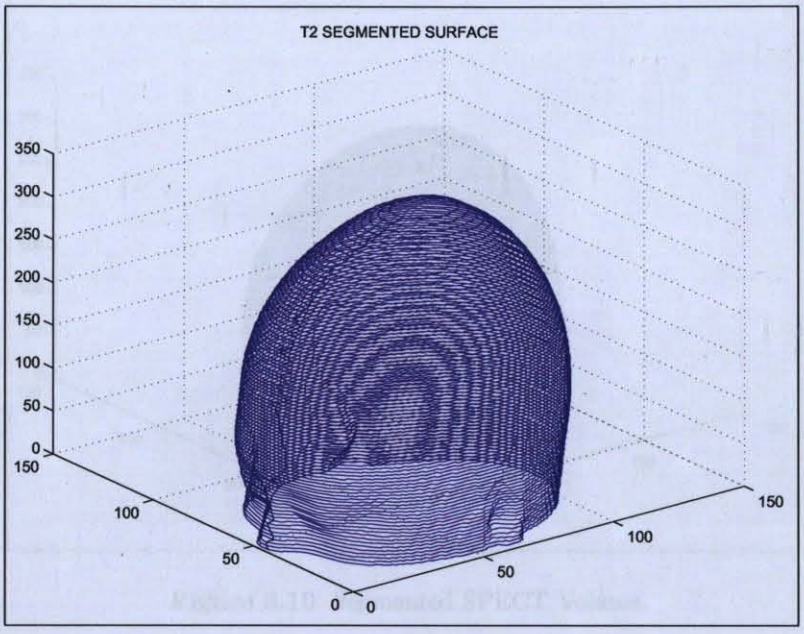

Figure 3.8 Segmented T2 Volume.

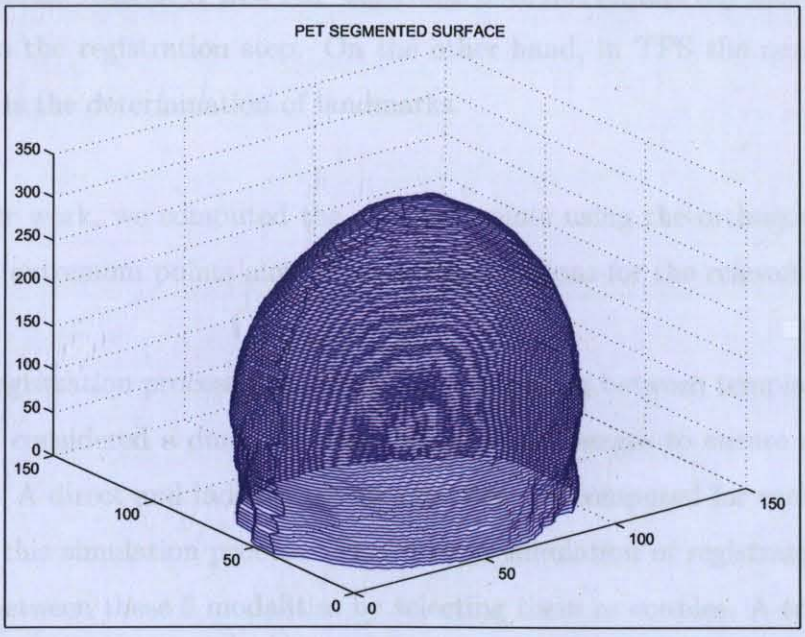

Figure 3.9 Segmented PET Volume.

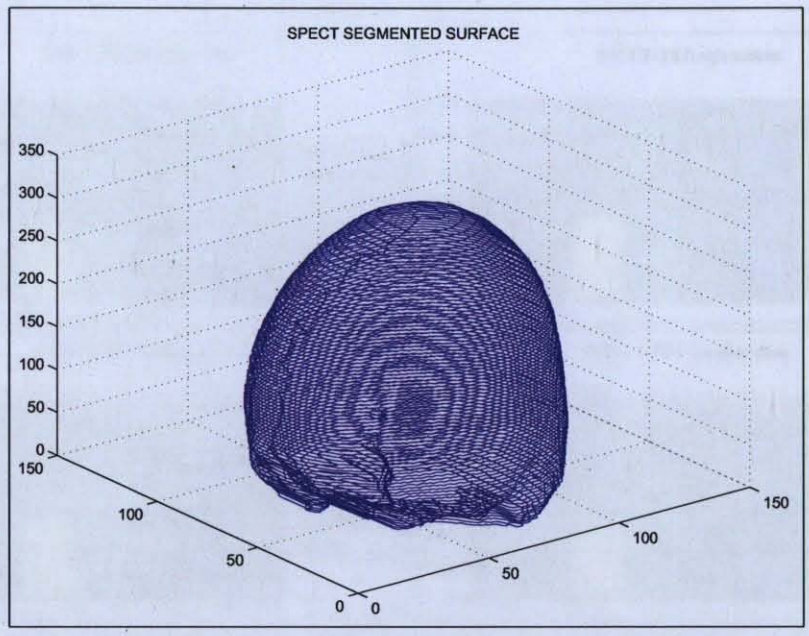

Figure 3.10 Segmented SPECT Volume.

3.8, 3.9 and 3.10 only surface points are visualized after the volume reconstruction is done.

We should remember that ICP algorithm does not require any more information to enter into the registration step. On the other hand, in TPS the next step before registration is the determination of landmarks.

In our work, we computed the extreme points using the orthogonal plane; we calculated 4 extremum points along $\pm$ x and y directions for the relevant slice.

All registration processes are based on a matching between template and target images. We considered a dual interpretation of these images to ensure a multimodal registration. A direct and indirect transformations are computed for each registration pair during this simulation process. Therefore, a simulation of registration study has been done between these 5 modalities by selecting them as couples. A transformation process tries to align images according to initial and final sets of points, hence we implemented this measurement with a dual approach and direct and reverse cases have been studied. (i.e. PET-T1 and T1-PET etc...)

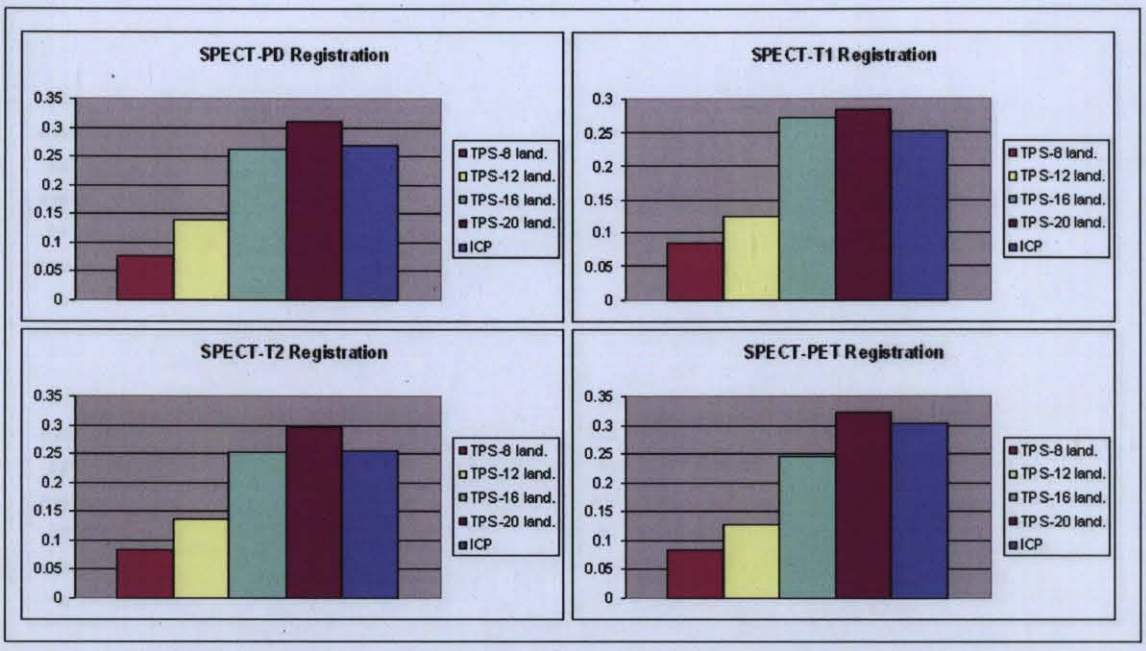

Figure 3.11 Graphical Representation of Table-1 where SPECT is Target Volume.

In order to increase the number of these pairwise measurements and especially to simulate the artifacts due to patient head movements along the gantry we needed to transform initial point sets in spherical coordinates by the means of rotation parameters. Firstly, we tried to rotate volumes between -20^o and $+20^o$ through θ and ϕ angles and by incrementing them with $+2^o$. This step of warping was meaningful to ensure our rotational deformations. Secondly, these rotated coordinates have been reset in cartesian coordinates. We note that our transformation parameters in ICP are compromising with x-, y- and z-axis. Even if the multimodal volumes had been rotated, they were close to each others. Especially their coordinates of center of gravity did not change drastically. For that purpose, all points sets required translation parameters. Finally, all rotated data coordinates have been translated through x-, y-, and z-axis by $+10$ units.

At the same time for TPS registration experiments we added a displacement noise on reference points. All TPS landmarks expressed in cartesian coordinates have been shifted in spherical coordinated by randomized displacement coefficients. θ and ϕ are defined between $[0-2\pi]$ and the distance or ***radius*** is set to 2 by default. These

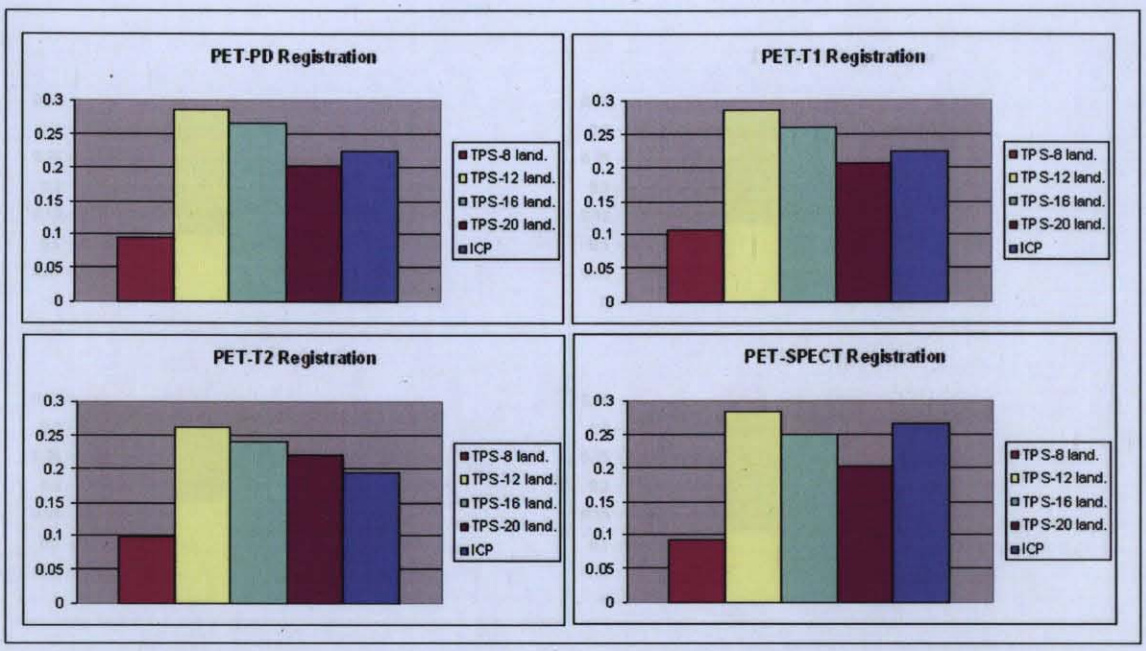

Figure 3.12 Graphical Representation of Table-1 where PET is Target Volume.

definition sets are multiplied by the generated random coefficient which is coming from the normal distribution and the final shifted landmark coordinates have been set. It is clear that this shifting is achieved for both template and target landmarks.

As a remark, we must note that we defined the unwarped (no translation, no rotation) data as '0' position. A registration process hasn't been occurred between point sets in 0 positions.

Totally, we obtained 20 target and 1 template (i.e. '0' state) volumes in each modality and a simulation process is computed for 400 different matchings that would be considered for both ICP and TPS.

Landmarks that figure out our reference points in TPS play a significant role in image registration. As a further step, we increased the landmark point number by a step size of 4. Finally we have done 4 different measurement for TPS; 8, 12, 16 and 20 landmarks. Each of them consisted of 400 registrations.

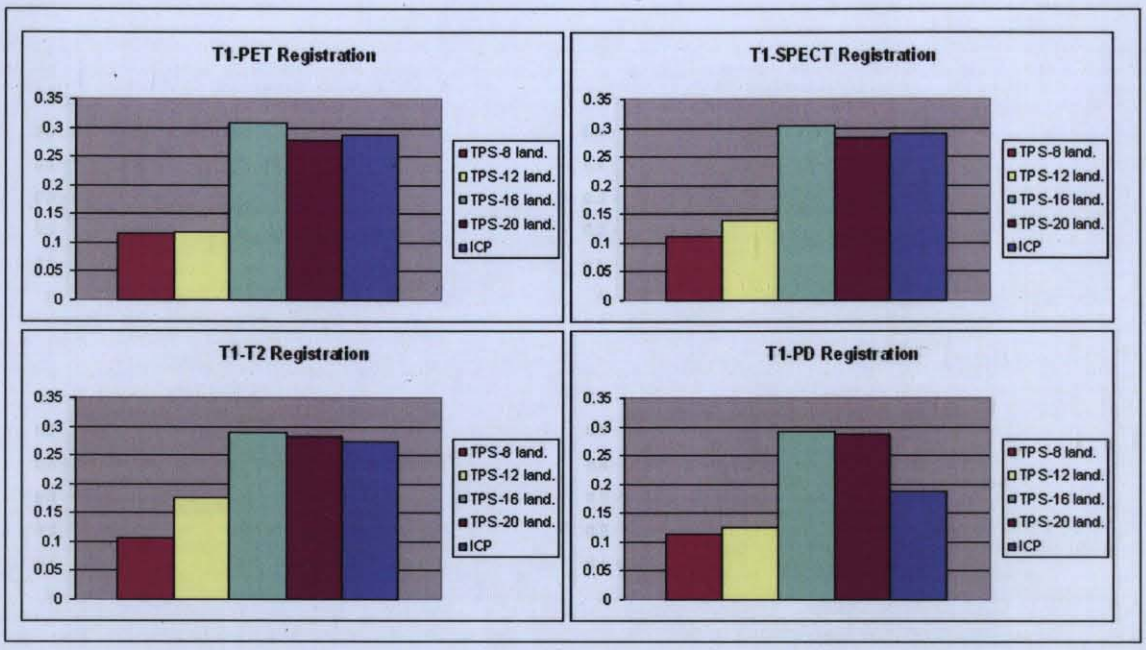

Figure 3.13 Graphical Representation of Table-1 where T1 is Target Volume.

Totally, for ICP we have done 400 measurements and for TPS we have done 1600 measurements with respect to landmark numbers.

All measurement results would be classified into 2 separated tables;

- Distance Difference Mean

$$Mean = \frac{\sum_{i=1}^{n} registered(i) - target(i)}{n} \tag{3.1}$$

- Root Mean Square :

$$R(x) = \sqrt{\frac{\sum_{i=1}^{n} x_i^2}{n}} \qquad \begin{array}{l} n : \textit{considered points or landmarks,} \\ x_i : \textit{distance difference between point pairs.} \end{array} \tag{3.2}$$

Representing 2000 measurements in these tables was meaningless due to registration's signification and table limitations. Therefore, we calculated an average value of 20 measurements for each modality in each registration procedure. As it is stated,

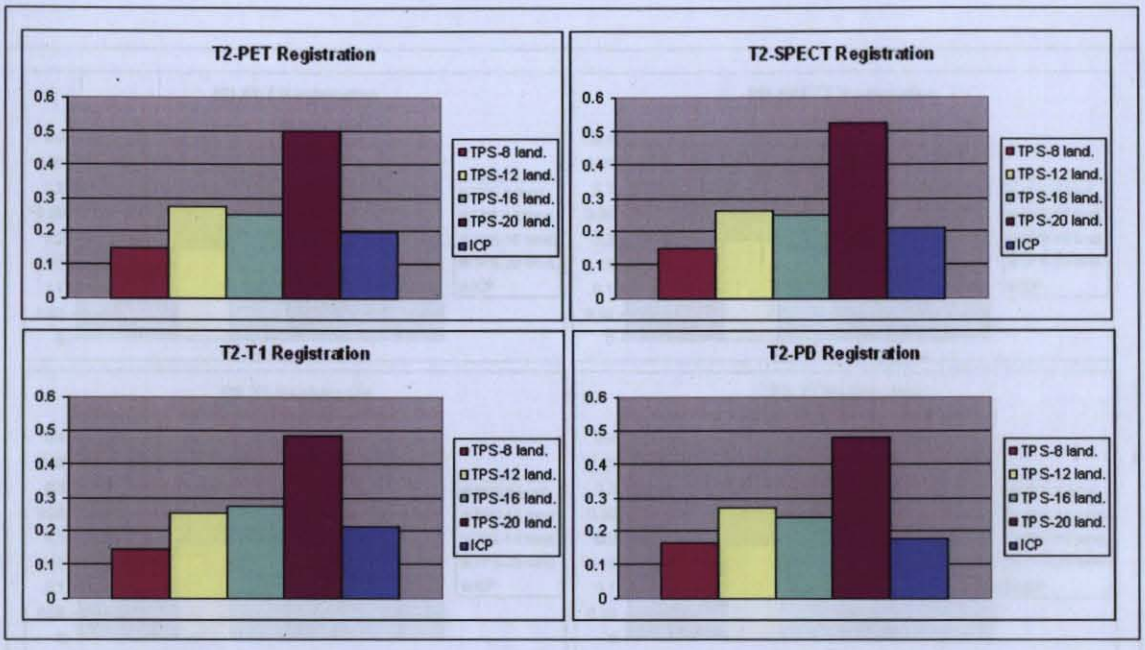

Figure 3.14 Graphical Representation of Table-1 where T2 is Target Volume.

we had 5 registration procedures; ICP, TPS-8 landmarks, TPS-12 landmarks, TPS-16 landmarks and TPS-20 landmarks. For each registration process, the value in Table-1 and Table-2 represents an average value of 20 coregistrations. The graphical representations of Table-1 and Table-2 are also given in Figures 3.11, 3.12, 3.13, 3.14, 3.15, 3.16, 3.17, 3.18, 3.19 and 3.20.

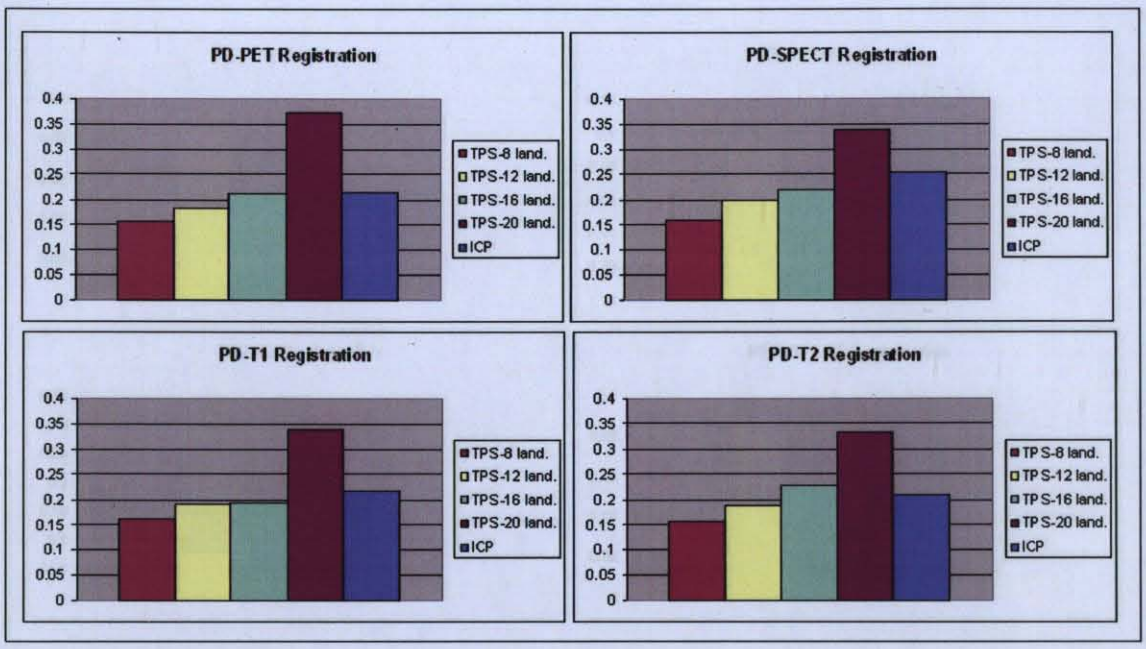

Figure 3.15 Graphical Representation of Table-1 where PD is Target Volume.

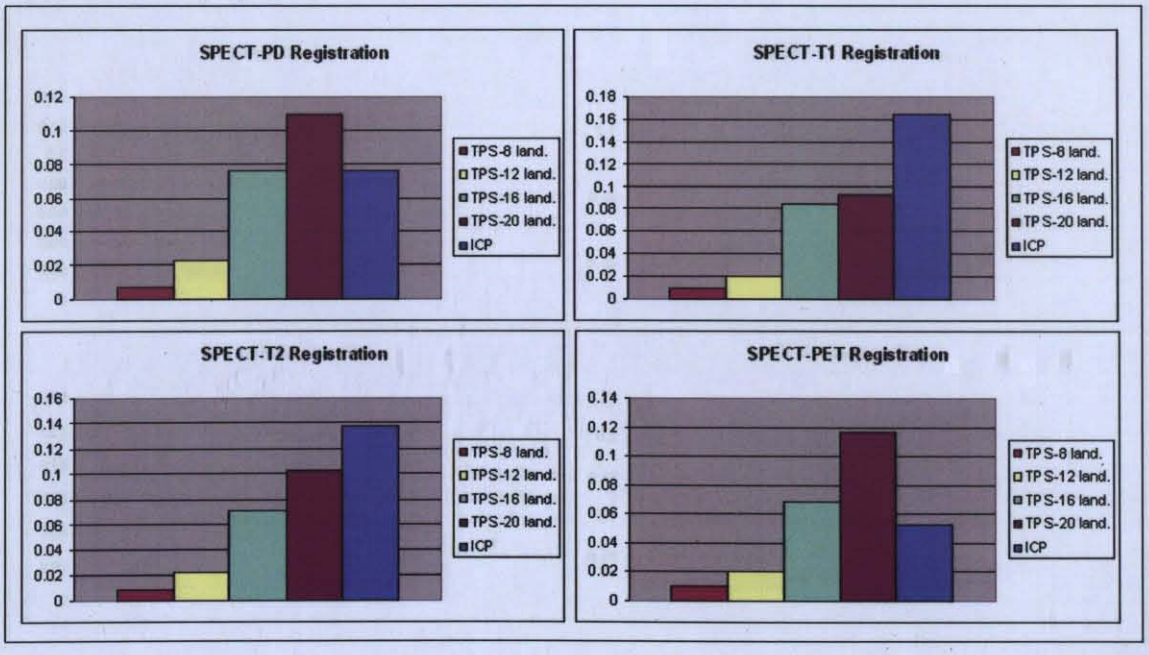

Figure 3.16 Graphical Representation of Table-2 where SPECT is Target Volume.

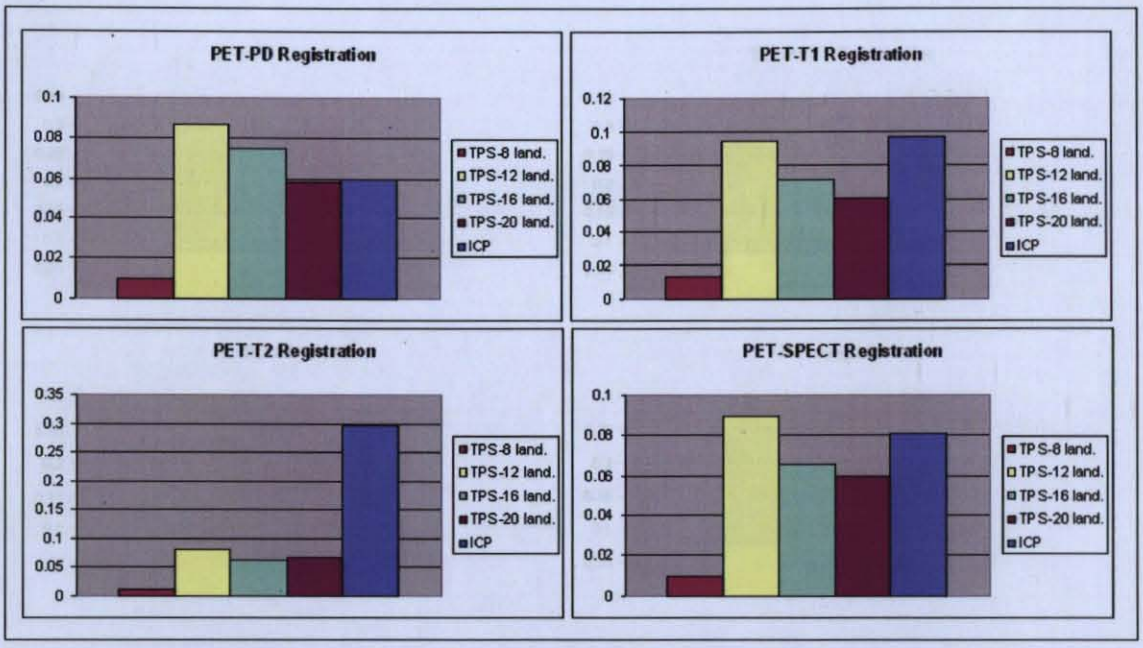

Figure 3.17 Graphical Representation of Table-2 where PET is Target Volume.

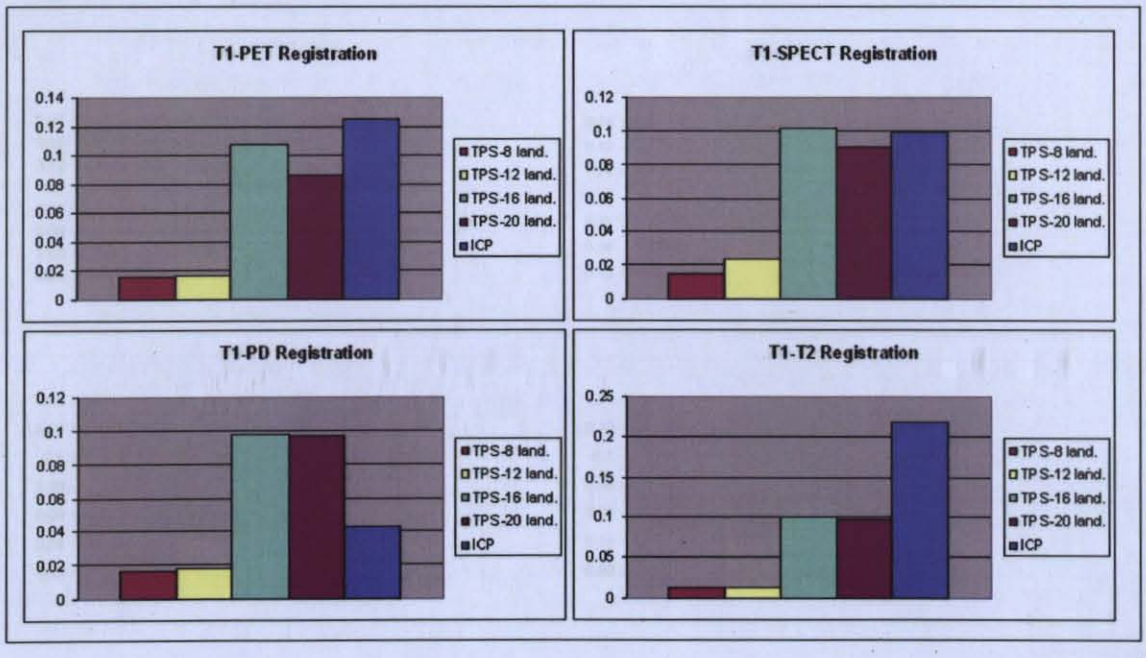

Figure 3.18 Graphical Representation of Table-2 where T1 is Target Volume.

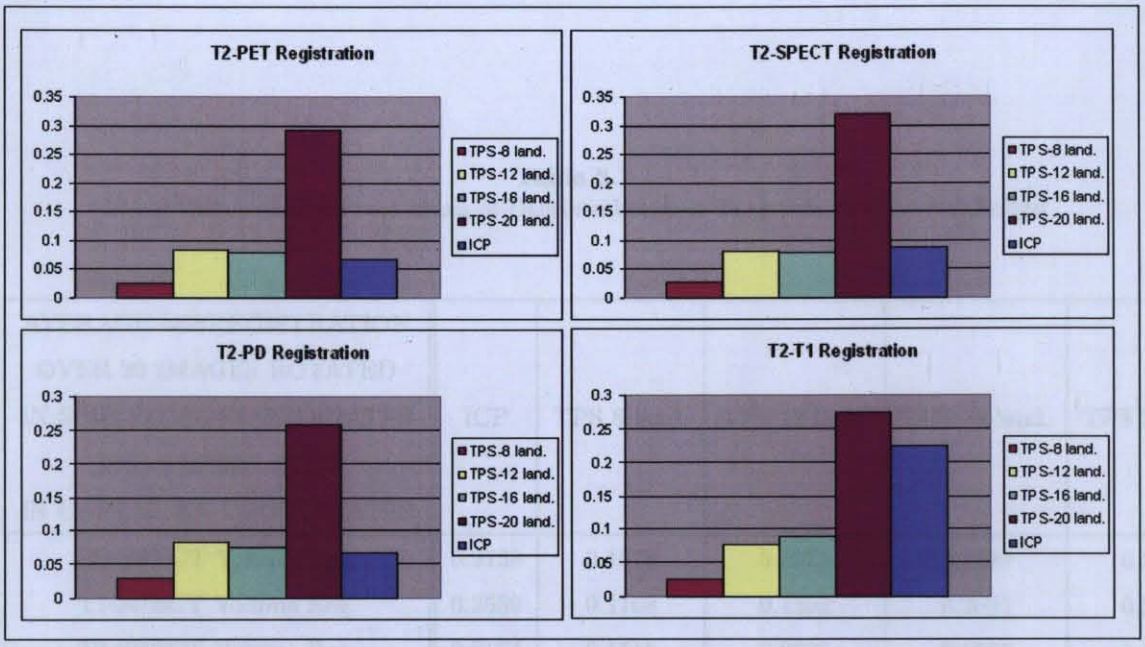

Figure 3.19 Graphical Representation of Table-2 where T2 is Target Volume.

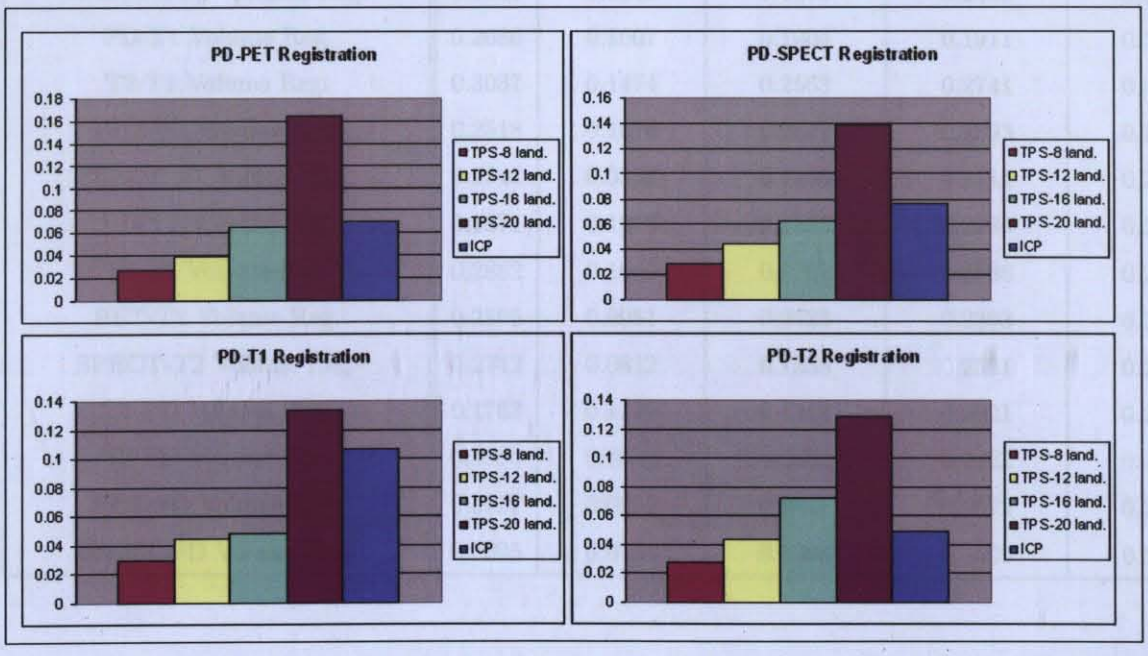

Figure 3.20 Graphical Representation of Table-2 where PD is Target Volume.

Table 3.1
Mean Values of Difference Mean of Distance between Target and Registered Points

AVERAGE MISREGISTRATION OVER 20 IMAGES ROTATED IN SPHERICAL COORDINATES AND TRANSLATED IN CARTESIAN COORDINATES	ICP	TPS 8 land.	TPS 12 land.	TPS 16 land.	TPS 20 land.
PD-SPECT Volume Reg.	0.2138	0.1578	0.1971	0.2187	0.3382
T1-SPECT Volume Reg.	0.2539	0.1108	0.1392	0.3037	0.2841
T2-SPECT Volume Reg.	0.2174	0.1515	0.2620	0.2525	0.5231
PET-SPECT Volume Reg.	0.2087	0.0928	0.2835	0.2500	0.2020
PD-PET Volume Reg.	0.2247	0.1558	0.1822	0.2105	0.3728
T1-PET Volume Reg.	0.2662	0.1146	0.1171	0.3063	0.2783
T2-PET Volume Reg.	0.2237	0.1500	0.2716	0.2514	0.5009
SPECT-PET Volume Reg.	0.1951	0.0845	0.1270	0.2446	0.3217
PD-T1 Volume Reg.	0.2686	0.1607	0.1904	0.1911	0.3384
T2-T1 Volume Reg.	0.3037	0.1474	0.2563	0.2741	0.4819
PET-T1 Volume Reg.	0.2518	0.1076	0.2847	0.2593	0.2056
SPECT-T1 Volume Reg.	0.2545	0.0852	0.1255	0.2711	0.2833
PD-T2 Volume Reg.	0.1871	0.1556	0.1883	0.2289	0.3340
T1-T2 Volume Reg.	0.2882	0.1059	0.1767	0.2886	0.2821
PET-T2 Volume Reg.	0.2895	0.0981	0.2623	0.2393	0.2208
SPECT-T2 Volume Reg.	0.2742	0.0812	0.1358	0.2521	0.2973
T1-PD Volume Reg.	0.1767	0.1139	0.1242	0.2921	0.2877
T2-PD Volume Reg.	0.1980	0.1629	0.2672	0.2422	0.4806
PET-PD Volume Reg.	0.2127	0.0952	0.2847	0.2672	0.2036
SPECT-PD Volume Reg.	0.2095	0.0756	0.1388	0.2606	0.3092

Table 3.2
Mean Values of Root Mean Square of Distance between Target and Registered Points

AVERAGE MISREGISTRATION OVER 20 IMAGES ROTATED IN SPHERICAL COORDINATES AND TRANSLATED IN CARTESIAN COORDINATES	ICP	TPS 8 land.	TPS 12 land.	TPS 16 land.	TPS 20 land.
PD-SPECT Volume Reg.	0.0756	0.0284	0.0443	0.0625	0.1383
T1-SPECT Volume Reg.	0.0989	0.0145	0.0235	0.1009	0.0903
T2-SPECT Volume Reg.	0.0880	0.0274	0.0804	0.0784	0.3195
PET-SPECT Volume Reg.	0.0809	0.0102	0.0892	0.0655	0.0594
PD-PET Volume Reg.	0.0689	0.0269	0.0388	0.0652	0.1648
T1-PET Volume Reg.	0.1248	0.0159	0.0160	0.1071	0.0858
T2-PET Volume Reg.	0.0668	0.0260	0.0820	0.0772	0.2912
SPECT-PET Volume Reg.	0.0522	0.0091	0.0203	0.0677	0.1168
PD-T1 Volume Reg.	0.1066	0.0293	0.0447	0.0473	0.1331
T2-T1 Volume Reg.	0.2250	0.0247	0.0771	0.0888	0.2736
PET-T1 Volume Reg.	0.0966	0.0132	0.0946	0.0713	0.0606
SPECT-T1 Volume Reg.	0.1653	0.00879	0.0190	0.0848	0.0929
PD-T2 Volume Reg.	0.0496	0.0277	0.0430	0.0722	0.1294
T1-T2 Volume Reg.	0.2180	0.0132	0.0123	0.1004	0.0961
PET-T2 Volume Reg.	0.2957	0.0110	0.07944	0.0607	0.0659
SPECT-T2 Volume Reg.	0.1373	0.0083	0.0224	0.0709	0.1031
T1-PD Volume Reg.	0.0429	0.0164	0.0181	0.0975	0.0964
T2-PD Volume Reg.	0.0675	0.0305	0.0828	0.0731	0.2577
PET-PD Volume Reg.	0.0591	0.0102	0.0866	0.0751	0.0579
SPECT-PD Volume Reg.	0.0762	0.0067	0.0231	0.0765	0.1101

4. DISCUSSION and CONCLUSION

Image Registration is a useful tool for matching different modalities that have complementary information about the considered objects. Registration is widely used ranging from remote sensing to robotics research. Registration is also needed to perform comparisons across a population, for deterministic and statistical atlas constructions and to merge anatomic and functional knowledge.

In our study, we intended to show the performance of two different algorithms; ICP and TPS to register multimodal images. In order to perform a 3-D simulation, it was indispensable to scale registration process and to determine sub-procedures. We divided our research into 3 steps; *segmentation*, *volume reconstruction* and *registration*.

Utilization of medical images somehow requires a segmentation process to extract the outer surface, or to analyze sub-anatomical regions. We need to get the surface information, especially the outer contour to set the surface information so-called the skull. Secondly we need to perform an image reconstruction to extrapolate 2-D coordinates in segmented slices.

In segmentation step, it was important to remember that the corresponding volumes; target and template volumes could be composed of different number of points. As the corresponding point sets can not be composed of the same field of view, their number of points could be different owing to surface extraction and image properties. In our multimodal study, we remarked that corresponding surfaces generally are composed of different surfaces.

Furthermore, as an intermediate step we calculated landmarks through the segmented polylines. This approach is called an *intrinsic registration* because the landmark information is extracted from the slices. It belongs to the respective anatomical features. However, as another method an *extrinsic registration* could be performed.

This requires physically inserted landmarks called as *fiducial markers*.

We determined these reference points by applying a semi-automatic method. Here, we realized our TPS measurements with 8, 12, 16 and 20 landmarks. These landmarks are automatically selected as the extreme points of slices positioned on Cartesian plane. On the other hand, for our measurements it can be enounced that if the landmark numbers increase the distance mean and RMS slightly increase. This is caused by the diffusion of the landmarks through the whole surface. When more landmarks are positioned, the energy minimization would not satisfy the previous cases and TPS method stops the convergence due to its mathematical formulation.

Finally, we applied our final step; registration procedure for all experimental protocols.

In our work, we intended to examine the efficiency of Thin-Plate Splines and Iterative Closest Point Methods in a multimodal approach. We considered two criteria; Distance Means and Root Mean Square Error Analysis in Table-1 and Table-2 respectively. In order to interpret the results and their corresponding meanings, we had to perform an evaluation in two steps;

1. A comparison between ICP and TPS.
2. The influence of landmark numbers in TPS.

In all measurements represented in Table 1 and 2 and also in the corresponding Figures 3.11, 3.12, 3.13, 3.14, 3.15, 3.16, 3.17, 3.18, 3.19 and 3.20, we found that TPS with 8 landmarks is better than ICP regarding of the distance minimization and correct alignment. However we noticed that as the landmark number increases the TPS efficiency decreases. When we compare TPS-20 landmarks with ICP registration, we conclude that ICP measurements are generally better. We observed that for distance difference means TPS gives better results at the range between 10^{-1} and 10^{-2} and for RMS the order is between 10^{-1} and 10^{-3}. On the other hand, in our simulation study

ICP alignment is $1.5-2$ times faster than TPS and warps the target onto the template without an extra requirement such as reference points or fiducial markers. Its only requirement is the settings of quaternion parameters and an adequate threshold value that the error function would iteratively converge.

It is clear that a decreasing in mean values signify better results as a means of closer points between the registered image and the template image have been established. In RMS tables the situation of the outputs is quite similar, however the orders are changed. Compendiously, we might infer that the utilization of ICP on skull surfaces would satisfy our requirements.

In studies of Lemieux et al. [34], Holden et al. [11] and Fright et al. [35], the RMS values are considered as the first comparison criterion. The efficiency of presented methods and corresponding results are measured according to RMS comparisons. In our study, we studied closest point pairs and distance differences according to mean of distance differences and RMS values.

For rigid anatomical features (especially skull and neurologic structures) or preprocessed and segmented slices, a global matching with ICP would be sufficient to achieve registration. By the way, it is clear that rigid transformations might be sufficient and could achieve a good matching especially in rigid areas such as skull and the relevant volume does not change spatially.

This *rigid body* assumption simplifies the registration process, but techniques that make this assumption have quite limited applicability. Many organs do deform substantially, for example with the cardiac or respiratory cycles or as a result of change in position. The brain within the skull is reasonably non-deformable provided, the skull remains closed between imaging, and that there is no substantial change in anatomy and pathology, such as growth in a lesion, between scans.

The main pitfall of ICP is to converge to the local minima. In our study, thanks to anatomical structures, ICP worked correctly. We also set good convergence levels

to prevent this local convergence. We aimed to decrease ICP computational time cost and combined our ICP implementation with computational functions derived from *K-D Tree Algorithm* which we have interested in also. However in cortical surfaces, cardiovascular studies, breast imaging or soft tissue analysis it is stated that the basic algorithm can converge to local minima and can cause misalignments. New approaches studied by Feldmar et al. [18] and Gelfand et al. [17] have reformulated ICP algorithm and its derivatives to prevent this wrong or local convergence.

ICP optimization can be accelerated by keeping track of the solutions at each iteration. As the algorithm iterates to the local minimum closest to the starting position, it may not find the correct match. The solution proposed by Besl and McKay [15] is to start the algorithm multiple times, each time with a different estimate of the rotation alignment, and to choose the minimum among the all minima obtained.

Though their landmark limitations, TPS could perform a registration but a specialist should determine the reference inputs or a trained method would perform the same process. The measurements described in Tables 1 and 2 show us that in each procedure, TPS gives us better results for 8 landmarks even if the images have been transformed and random noise has been added on landmark coordinates. On the other hand, we found that when landmark numbers have increased the TPS efficiency has decreased. By the way, with respect to computational time cost, ICP is also faster than TPS. In summary ICP gave us fast and reliable results on skull surfaces without extra information as landmarks.

Although a lot of research has been done, automatic image registration remained as an open problem. Registration of images with complex nonlinear and local distortions, multimodal registration and registration of N-D images (where $N > 2$) belong to the most challenging tasks at this moment.

When registering images with nonlinear approaches, we are faced with two basic problems;

1. How to match the control points.

2. Which mapping functions to use for registration.

While the second one can be solved at least on theoretical level by using appropriate radial basis functions, the first problem is generally unsolvable due to its nature. Since the between-image deformations can be arbitrary, we cannot use any automatic matching method. Another conceptual question here is how can we distinguish between image deformations and real changes of the target.

In a further study, it would be useful to visualize the entire volume in order to locate our landmarks into the brain compartments and cortical surface. On the contrary, as described above before cortical surface determination and internal (brain) registration we would necessitate dedicated segmentation algorithms to find out these finest landmarks. Generally, the locations and landmark numbers depend on the application area. However, due to the complexity of cortical surface, an internal registration will require numerous landmarks. As a deduction we might infer that the complexity of anatomical surfaces is compromising with landmark numbers.

As future work, Image Registration could be extended to image fusion. As we remark, different modalities possess different information. An alignment process could only match different modalities according to their morphological characteristics or their image pixels/voxels information. However it does not either combine or superimpose that information. On the other hand, to ensure a complete mixture, another tool should be studied. Image fusion is a multi-level process that requires a segmentation and a registration step. A segmentation serves to extract the required information that will be one of the parameters, the other one is the landmarks or the location parameters such as rotation angles or translation distances. Secondly, a registration should be maintained to achieve a global or local matching depending on the selected area. Finally, the collected data coming from the previous process serve to mix up the information into a global image.

APPENDIX A. Mathematical Foundations

A.1 Iterative Closest Point

A.1.1 Definition of Point Sets

N_p and N_x are the number of points in sets P, X;

$$P = \{p_i\} \qquad i = 1, \cdots, N_p \tag{A.1}$$

$$X = \{x_i\} \qquad i = 1, \cdots, N_x \tag{A.2}$$

p_i and x_i are 3-D vectors;

$$x_i = \begin{bmatrix} x_i & y_i & z_i \end{bmatrix} \tag{A.3}$$

Evaluation of the distance between a point and a data set is denoted by $d(p_i, X)$:

$$d(p_i, X) = \min_{j \in \{1, \cdots, N_x\}} d(p_i, x_j) \tag{A.4}$$

The set Y of closest points is calculated, the corresponding process is denoted by the operator C:

$$Y = C(P, X) \tag{A.5}$$

where $Ny = Np$.

A.1.2 Quaternions

Quaternions are a means of representing 3-D rotations. A unit quaternion is a 4-D vector $q_R = \begin{bmatrix} q_0 & q_1 & q_2 & q_3 \end{bmatrix}^T$ that satisfies $q_0 \geq 0$ and $q_0^2 + q_1^2 + q_2^2 + q_3^2 = 1$. Rotation by an angle θ around a unit vector $[x_1\ x_2\ x_3]^T$;

$$q_R = \begin{bmatrix} \cos\frac{\theta}{2} & x_1 \sin\frac{\theta}{2} & x_2 \sin\frac{\theta}{2} & x_3 \sin\frac{\theta}{2} \end{bmatrix}^T \tag{A.6}$$

The rotation matrix **R** that corresponds to a certain quaternion;

$$R(q_R) = \begin{bmatrix} q_0^2 + q_1^2 - q_2^2 - q_3^2 & 2(q_1q_2 - q_0q_3) & 2(q_1q_3 + q_0q_2) \\ 2(q_1q_2 + q_0q_3) & q_0^2 + q_2^2 - q_1^2 - q_3^2 & 2(q_2q_3 - q_0q_1) \\ 2(q_1q_3 - q_0q_2) & 2(q_2q_3 + q_0q_1) & q_0^2 + q_3^2 - q_1^2 - q_2^2 \end{bmatrix} \tag{A.7}$$

A 3-D translation is defined by $q_T = \begin{bmatrix} q_4 & q_5 & q_6 \end{bmatrix}^T$. Two vectors are combined in a single **registration vector: q**.

$$q = \begin{bmatrix} q_R \\ q_T \end{bmatrix} = \begin{bmatrix} q_0 & q_1 & q_2 & q_3 & q_4 & q_5 & q_6 \end{bmatrix}^T \tag{A.8}$$

The optimal registration vector is the one that minimizes the following mean square error function:

$$f(q) = \frac{1}{N_p} \sum_{i=1}^{N_p} \|y_i - R(q_R)p_i - q_T\|^2 \tag{A.9}$$

A.2 Thin Plate Splines

A.2.1 Radial Basis Function Splines

Radial basis function splines are defined as a linear combination of n radial basis functions $\theta(s)$;

$$\phi(x,y,z) = a + b_x x + b_y y + b_z z + \sum_{k=1}^{n} w_k \theta(|\psi_j - (x,y,z)|) \quad \text{(A.10)}$$

$$\phi(x,y,z) = a + b_x x + b_y y + b_z z + \sum_{k=1}^{n} w_k g(\sqrt{(x-x_k)^2 + (y-y_k)^2 + (z-z_k)^2}) \quad \text{(A.11)}$$

Radial basis functions are defined;

$$\theta(r) = \begin{cases} |r|^2 \log(|r|) & \text{in 2D,} \\ |r| & \text{in 3D.} \end{cases} \quad \text{(A.12)}$$

A.2.2 Statement of Registration Problem

Let $K_i = Q_i - P_i$ $i \in \{1, \cdots, n\}$ where Q and P are template and target landmarks and n is the total number of landmarks.

K_i depicts the displacement between corresponding landmarks.

$$\begin{bmatrix} K_1 \\ K_2 \\ \vdots \\ K_N \end{bmatrix} = \begin{bmatrix} \sum_{k=1}^{n} w_k U(p_1 - p_k) + a + b_x q_{1x} + b_y q_{1y} + b_z q_{1z} \\ \sum_{k=1}^{n} w_k U(p_2 - p_k) + a + b_x q_{2x} + b_y q_{2y} + b_z q_{2z} \\ \vdots \\ \sum_{k=1}^{n} w_k U(p_n - p_k) + a + b_x q_{nx} + b_y q_{ny} + b_z q_{nz} \end{bmatrix} \quad \text{(A.13)}$$

The variation function of Thin-Plate Spline is defined in a matrix form;

$$\phi(\vec{v}) = a + \vec{b}^T \vec{v} + W^T \vec{g}(\vec{v}) \quad \text{(A.14)}$$

where

$$\vec{v} = \begin{bmatrix} x \\ y \\ z \end{bmatrix} \qquad \vec{b} = \begin{bmatrix} b_x \\ b_y \\ b_z \end{bmatrix} \qquad W = \begin{bmatrix} w_1 \\ w_2 \\ w_3 \end{bmatrix} \tag{A.15}$$

and

$$\vec{g}(x,y,z) = \begin{bmatrix} \sqrt{(x-x_1)^2+(y-y_1)^2+(z-z_1)^2} \\ \sqrt{(x-x_2)^2+(y-y_2)^2+(z-z_2)^2} \\ \vdots \\ \sqrt{(x-x_n)^2+(y-y_n)^2+(z-z_n)^2} \end{bmatrix} \tag{A.16}$$

The following constraints are imposed in order to allow minimal energy.

$$\sum w_k = \sum w_k x_k = \sum w_k y_k = \sum w_k z_k \quad . \tag{A.17}$$

APPENDIX B. Computational Application and Format of Provided Disc

The computational application and source codes are provided with a Compact Disc (CD). In this disc, we divided our study into three folders; Iterative Closest Point Algorithm Application, 3-D Thin-Plate Splines Application and Example Files from our Simulation Study.

B.1 Preliminary functions

Slice_contour function calculates the contour information of the selected slice in 2-D.

The parameters are;

- I = selected slice.
- output = 2D coordinates of the selected slice contour.

Add_noise_on_landmarks function adds random noise with respect to Normal distribution on point landmarks distributed onto the skull surface. This noise is added on both template and target reference points.

B.2 ICP Folder

In this folder, we have listed functions related with Iterative Closest Point Algorithm;

B.2.1 ICP function

This function performs the registration of 3D points with respect to template using ICP algorithm.

The inputs are;

- model ($mx3$) = set of template points.
- pts ($nx3$) = set of target points.
- flag = control parameter; it has two states: 'off' : nothing displayed on screen. 'on' : information displayed on screen while iteration is taking place.

The outputs are;

- ptsnew = registered points.
- Rnew = rotation matrix calculated by ICP Algorithm.
- vtnew = translation matrix calculated by ICP Algorithm.

The inner function **update** located in the same function performs the update when the algorithm prepares the next iteration.

B.2.2 Dist function

This function calculates the Euclidean 3-D distance between two inputs x, y. The output of this function is needed for other functions.

B.2.3 Mean_Rms function

This function performs the evaluation of the registration results through the formulation of distance differences. The mean values and the corresponding Root-Mean Square measurements can be obtained via this function.

The inputs are;

- target = target point sets.
- registered = registered point sets.

The outputs are;

- moyenne = mean value of distance differences between target and registered point sets.
- rms = root mean square value of distance differences between target and registered point sets.

B.2.4 Stdevicp function

This function perform a Standard Deviation Analysis of Distance Differences between Target and Registered point sets.

B.2.5 Drawing function

This function draws the template, target and registered points sets using mesh and 3-D plots. The inputs are 20 volumes of the simulation study.

B.3 TPS Folder

In this folder, we have listed functions related with 3-D Thin Plate Splines Method;

B.3.1 Base function

A 3-D radial basis function of our Thin-Plate Splines is set here. We calculate the output *result* through the value that we set with *ro*.

B.3.2 Thinplate function

This function calculates a pair of Thin-Plate Splines that represent this elastic transformation.

The inputs are;

- S = Input points.
- Q = Control points.

The outputs are;

- C2 = The target function of Thin-Plate Splines.
- E = Bending energy of Thin-Plate Splines.

B.3.3 Evaltps function

This function finds the singular value decomposition to solve the equations and calculate the transformed image (i.e. registered point sets).

The inputs are;

- S = Template control points.
- params = Target function of Thin-Plate Splines.
- S = Target control points.

The outputs are;

- C2 = Final form of transformed points.

B.3.4 Dist function

This function calculates the Euclidean 3-D distance between two inputs x, y. The output of this function is needed for other functions. This function is similar to the file in ICP folder.

B.3.5 Mean_Rms function

This function performs the evaluation of the registration results through the formulation of distance differences. The mean values and the corresponding Root-Mean Square measurements can be obtained via this function. This function is similar to the file in ICP folder.

B.3.6 Drawing function

This function draws the template, target and registered points sets using mesh and 3-D plots. The inputs are 20 volumes of the simulation study. This function is similar to the file in ICP folder.

B.4 Examples from Multimodal Registration

In this folder, several MATLAB files have been introduced. In order to run these files some data files with .mat extensions are also provided. At the same folder, noisy and raw data files are provided.

As an example file like *PDPET-tps16.m*, we perform a TPS based registration with 16 landmarks. Our template image is PD-weighted MR volume and the target image is PET. We can analyze the output; registered volume via other functions and also plot it.

REFERENCES

1. Brown, L., "A survey of image registration techniques," *ACM Computing Surveys*, Vol. 24, no. 4, pp. 325–366, 1992.

2. Besl, P. J., "Geometric modeling and computer vision," *Proceedings of the IEEE*, Vol. 76, pp. 936–958, August 1988.

3. Szeliski, R., and J. Coughlan, "Spline-based image registration," *International Journal of Computer Vision*, Vol. 22, no. 3, pp. 199–218, 1997.

4. Ozturk, C., A. Derbyshire, and E. McVeigh, "Estimating motion from mri data," *Proceedings of the IEEE*, Vol. 91, no. 10, pp. 1627–1647, 2003.

5. Stokking, R., K. Zuiderveld, and M. Viergever, "Integrated volume visualization of functional image data and anatomical surfaces using normal fusion," *Human Brain Mapping*, no. 12, pp. 203–218, 2001.

6. Sturm, B., K. Powell, A. Stillman, and R. D. White, "Registration of 3d ct angiography and cardiac mr images in coronary artery disease patients," *The International Journal of Cardiovascular Imaging*, Vol. 19, pp. 281–293, 2003.

7. Rusinek, H., A. Levy, and M. E. Noz, "Performance of two methods for registering pet and mr brain scans," *Nuclear Science Symposium and Medical Imaging Conference*, Vol. 3, pp. 2159–2162, 2-9 November 1991.

8. Glozman, D., M. Shoham, and A. Fischer, "A surface-matching technique for robot-assisted registration," *Computer Aided Surgery*, Vol. 6, pp. 259–269, 2001.

9. Chen, Y., and M. Wang, "3d reconstruction and fusion for multi-modality spinal images," *Computerized Medical Imaging and Graphics*, pp. 1–11, 2003.

10. Nyúl, L., and J. Udupa, "Incorporating a measure of local scale in voxel-based 3-d image registration," *IEEE Transactions on Medical Imaging*, Vol. 22, no. 2, pp. 228–237, 2003.

11. Holden, M., L. Hill, E. Denton, J. Jarosz, T. Cox, T. Rohlfing, J. Goodley, and D. Hawkes, "Voxel similarity measures for 3-d serial mr brain image registration," *IEEE Transactions on Medical Imaging*, Vol. 19, no. 2, pp. 94–102, 2000.

12. Zhu, Y. M., and S. Cochoff, "Likelihood maximization approach to image registration," *IEEE Transactions on Image Processing*, Vol. 11, no. 12, pp. 1417–1426, 2002.

13. Rohlfing, T., J. West, J. Beier, T. Liebig, C. Taschner, and U. Thomale, "Registration of functional and anatomical mri: Accuracy assesment and application in navigated neurosurgery," *Computer Aided Surgery*, no. 5, pp. 414–425, 2000.

14. Fischer, B., and J. Modersitzki, "Combining landmark and intensity driven registrations," *PAMM - Proc. Appl. Math. Mech.*, no. 3, pp. 32–35, 2003.

15. Besl, P., and N. McKay, "A method for registration of 3 - d shapes," *IEEE Transactions on Pattern Analysis and Machine Intelligence*, Vol. 14, no. 2, pp. 239–256, 1992.

16. Greenspan, M., and M. Yurick, "Approximate k-d search for efficient icp," *Proceedings of the Fourth International Conference on 3-D Digital Imaging and Modeling (3DIM'03)*, 2003.

17. Gelfand, N., L. Ikemoto, S. Rusinkiewicz, and M. Levoy, "Geometrically stable sampling for the icp algorithm," *Proceedings of the Fourth International Conference on 3-D Digital Imaging and Modeling (3DIM'03)*, 2003.

18. Feldmar, J., G. Malandain, J. Declerck, and N. Ayache, "Extension of the icp algorithm to non-rigid intensity-based registration of 3 - d volumes," *Proceedings of MMBIA '96*, pp. 84–93, 1996.

19. Szeliski, R., and S. Lavallée, "Matching 3-d anatomical surfaces with non-rigid deformations using octree-splines," *Proceedings of the IEEE Workshop on Biomedical Image Analysis*, pp. 144–153, 24-25 June 1994.

20. Hamadeh, A., S. Lavallée, R. Szeliski, P. Cinquin, and O. Péria, *Anatomy-based Registration for Computer-integrated surgery*, Vol. 905 of *Lecture Notes in Computer Science*, pp. 212–218. Nice-France: Springer-Verlag, April 1995.

21. Maintz, J. B., P. A. Elsen, and M. A. Viergever, *Comparison of Feature-Based Matching of CT and MR Brain Images*, Vol. 905 of *Lecture Notes in Computer Science*, pp. 219–228. Nice-France: Springer-Verlag, April 1995.

22. Bookstein, F., "Principal warps: Thin-plate splines and the decomposition of deformations," *IEEE Transactions on Pattern Analysis and Machine Intelligence*, Vol. 11, no. 6, pp. 567–585, 1989.

23. Christensen, G., and H. Johnson, "Consistent image registration," *IEEE Transactions on Medical Imaging*, Vol. 20, no. 7, pp. 568–582, 2001.

24. Lewis, J., H. J. Hwang, U. Neumann, and R. Enciso, "Smart point landmark distribution for thin-plate splines," *SPIE Medical Imaging*, Vol. 5370, pp. 1236–1243, 2004.

25. Rohr, K., H. Stiehl, R. Sprengel, W. Beil, T. Buzug, J. Weese, and M. Kuhn, *Point-Based Elastic Registration of Medical Image Data Using Approximating Thin-Plate Splines*, pp. 297–306. Visualization in Biomedical Computing, Springer-Verlag, 1996.

26. Rohr, K., M. Fornefett, and H. Stiehl, *Approximating Thin-Plate Splines for Elastic Registration: Integration of Landmark Errors and Orientation Attributes*, Vol. 1613 of *Lecture Notes in Computer Science*, pp. 252–265. Visegrad-Hungary: Springer-Verlag, June/July 1999.

27. Rohr, K., "Landmark-based elastic matching of 3d medical images," *Second Germany-Korea Joint Conf. on Advanced Medical Image Processing*, pp. 60–63, June 19-24 1997.

28. Rohr, K., and H. Stiehl, "Characterization and localization of anatomical landmarks in medical images," *Proc. 1st Aachen Conf. on Neuropsychology in Neurosurgery, Psychiatry, and Neurology*, pp. 9–12, Dec. 12-14 1997.

29. Rohr, K., H. Stiehl, R. Sprengel, T. Buzug, J. Weese, and M. Kuhn, "Landmark-based elastic registration using approximating thin-plate splines," *IEEE Transactions on Medical Imaging*, Vol. 20, no. 6, pp. 526–534, 2001.

30. Rohr, K., "Spline - based elastic image registration," *PAMM - Proc. Appl. Math. Mech.*, no. 3, pp. 36–39, 2003.

31. Elsen, P. A., L. Zelfde, and M. A. Viergever, "Near-automatic detection of arrow-shaped markers," *11th IAPR International Conference on Pattern Recognition, VOL I. Conferenece A : Computer Vision and Applications*, pp. 755–759, 30 August-3 September 1992.

32. Tan, I., R. van Schijndel, M. van Walderveen, M. Quist, R. Bos, P. Pouwels, P. Desmedt, H. Ader, and F. Barkhof, "Magnetic resonance image registration in multiple sclerosis: Comparison with repositioning error and observer-based variability," *Journal of Magnetic Resonance Imaging*, pp. 505–510, 2002.

33. Hsu, L., M. Loew, and J. Ostuni, "Automated registration of brain images using edge and surface features," *IEEE Engineering in Medicine and Biology*, pp. 40–47, 1999.

34. Lemieux, L., U. C. Wieshmann, N. F. Moran, D. R. Fish, and S. D. Shoovon, "The detection and significance of subtle changes in mixed signal brain lesions by serial mri scan matching and spatial normalization," *Medical Image Analysis*, Vol. 2, no. 3, pp. 227–242, 1998.

35. Fright, W., and A. Linney, "Registration of 3-d head surfaces using multiple landmarks," *IEEE Transactions on Medical Imaging*, Vol. 12, no. 3, pp. 515–520, 1993.

36. Hajnal, J., D. Hill, and D. Hawkes, *Medical Image Registration*, CRC Press, 2001.

37. Maguire, G., M. Noz, H. Rusinek, J. Jaeger, E. Kramer, J. Sanger, and G. Smith, "Graphics applied to medical image registration," *IEEE Computer Graphics and Applications*, pp. 20–28, 1991.

38. Moshfeghi, M., S. Ranganath, and K. Nawyn, "3d elastic matching of volumes," *IEEE Transactions on Image Processing*, Vol. 3, no. 2, pp. 128–138, 1994.

39. Elsen, P., E.-J. Pol, and M. Viergever, "Medical image matching - a review with classification," *IEEE Engineering in Medicine and Biology*, pp. 26–39, 1993.

40. Bloch, I., and H. Maître, "Data fusion in 2-d and 3-d image processing: An overview," *Proceedings of X. Brazilian Symposium on Computer Graphics and Image Processing*, pp. 127–134, 14-17 October 1997.

41. Hemler, P., T. Sumanaweera, P. A. Elsen, S. Napel, and J. Adler, "A system for multimodality image fusion," *Proceedings of IEEE 7th Syposium on Computer-Based Medical Systems*, pp. 335–340, 10-12 June 1994.

42. Thévenaz, P., U. Ruttimann, and M. Unser, "Iterative multi-scale registration without landmarks," *IEEE International Conference on Image Processing*, Vol. 3, pp. 228–231, 23-26 October 1995.

43. Terzopoulos, D., and A. W. Schlumberger, "Physically based models with rigid and deformable components," *IEEE Computer Graphics and Application*, pp. 41–51, 1988.

44. Kim, B., K. A. Frey, S. Mukhopadhyay, B. D. Ross, and C. R. Meyer, *Co-Registration of MRI and Autoradiography of Rat Brain in Three-Dimensions Following Automatic Reconstruction of 2D Data Set*, Vol. 905 of *Lecture Notes in Computer Science*, pp. 262–267. Nice-France: Springer-Verlag, April 1995.